NATIONAL ADVISORY COMMITTEE FOR AERONAUTICS

TECHNICAL NOTE 3032

AN ANALYTICAL STUDY OF THE EFFECT OF AIRPLANE WAKE ON THE LATERAL DISPERSION OF AERIAL SPRAYS

By Wilmer H. Reed, III

Langley Aeronautical Laboratory
Langley Field, Va.

Washington
October 1953

NATIONAL ADVISORY COMMITTEE FOR AERONAUTICS

TECHNICAL NOTE 3032

AN ANALYTICAL STUDY OF THE EFFECT OF AIRPLANE WAKE ON THE LATERAL DISPERSION OF AERIAL SPRAYS

By Wilmer H. Reed, III

SUMMARY

Calculations are made to determine the trajectories of liquid droplets introduced into the air disturbances generated by an airplane engaged in aerial spraying. The effects of such factors as the position at which droplets are ejected into the disturbances, airplane lift coefficient, and altitude are investigated. The distribution of deposit on the ground is computed for several droplet-size spectra, variations in the rate at which mass is ejected along the span, and lateral flight-path spacings. Consideration is then given to the problem of adjusting these factors with the aim of improving the uniformity and increasing the effective width of the deposit.

The results indicate that the lateral dispersion of droplets is increased when the spanwise position at which particles are ejected is moved toward the wing tip. Greater dispersion also results when the airplane lift coefficient or altitude is increased.

With the spray discharged continuously along the span at a constant rate, the deposit has a maximum concentration at the plane of symmetry, and rapidly diminishing concentration beyond the wing tip. In such cases, it was found that the uniformity and effective width of the swath could be improved by increasing the mass efflux rate with spanwise distance from the center line of the wing. When this is done, the lateral distance between adjacent flight paths required for a given degree of uniformity shows an increase amounting to from 0.4 to 1.0 semispan. Of the two droplet-size spectra considered, the one having the smaller mean diameter (200 microns) gives a more uniform deposit for a given flight-path spacing and the degree of uniformity is less sensitive to changes in the spacing of adjacent passes of the airplane.

INTRODUCTION

Although airplanes have been used to disperse liquid sprays and dust for insect control and agricultural purposes for many years, only

recently has an appreciable amount of study been devoted to the problem of improving the efficiency and effectiveness of the operation. One of the problems recognized as being important is that of obtaining a suitable distribution of the deposit. Experimental studies made by the Forest Insect Laboratory of Beltsville, Maryland (ref. 1) have indicated that, in general, aerial spray deposits exhibit excessive peaks of concentration beneath the airplane with diminishing intensity toward the outer edge of the swath. Although it is possible to improve these measured deposit characteristics by a tedious trial-and-error process, it is believed that a theoretical study of the important physical factors involved would provide a better understanding of the mechanism which determines the lateral dispersion of particles ejected into the flow field behind an airplane. Such a study may also suggest possible methods of improving the deposit characteristics which might otherwise be overlooked.

In the present paper the paths of liquid spray droplets issued into the flow field behind an airplane are calculated. Considered in these computations are the effects of such factors as the droplet-size spectrum, spanwise location of nozzles, height of airplane above the ground, and aerodynamic flow field in the wake. Distributions of deposit are determined for several variations of these parameters, with a view to improving the uniformity and the effective width of the swath. The airplane used as an illustration in the analysis is the agricultural prototype designated the Ag-1.

SYMBOLS

A	wing aspect ratio
b	wing semispan, ft
C	concentration of deposit, lb/Unit area
C_D	drag coefficient of droplet
C_L	lift coefficient of airplane
D	drag force on droplet, lb
δ	diameter of droplet, microns (1 micron = 3.28×10^{-6} ft)
δ_m	mean diameter of droplets, microns
g	acceleration due to gravity, ft/sec^2
m	mass of droplet, slugs

$$P = \frac{1}{y_g - y_0}$$

Q	mass ejected per unit length along flight path, lb/Unit length
q	velocity induced by isolated rectilinear vortex, ft/sec
R	Reynolds number of droplet
R_U	Reynolds number of droplet moving through still air at velocity U
r	radial distance from vortex center, ft
t	time, sec
U	flight velocity, ft/sec
v	percent of total volume
v_a, w_a	velocity components of air in y- and z-direction, respectively, ft/sec
v_d, w_d	velocity components of droplet in y- and z-direction, respectively, ft/sec
x,y,z	longitudinal, lateral, and vertical coordinates of droplet, respectively, semispans
z'	vertical coordinate of droplet with origin shifted to the bound vortex, semispans
α	dimensionless parameter, $\frac{\sigma C_D R_t}{24 R_U}$
Γ	circulation, ft^2/sec
ϵ	dispersion of droplet diameters, microns
η,ζ	lateral and vertical coordinates of trailing vortex cores, semispans
μ	absolute viscosity of air, slugs/ft-sec
ν	kinematic viscosity of air, ft^2/sec

ρ_a density of air, slugs/cu ft

ρ_d density of droplets, slugs/cu ft

σ dimensionless parameter, $18 \frac{b}{\delta} \frac{\rho_a}{\rho_d}$

τ dimensionless time, Ut/b

Subscripts:

0 initial value

g intersection of droplet path with ground plane

y,z lateral and vertical directions, respectively

t terminal velocity of droplet

c correction due to bound vortex

ANALYSIS

The paths taken by spray droplets issued from an airplane are influenced by the flow field induced in the region of air through which the airplane has flown. When drag forces acting on the droplets are predominant, as in the case of small particles, the trajectories follow the streamlines of flow more closely than do the trajectories of larger particles for which inertia forces are predominant. In aerial sprays, the smallest particles may remain in suspension in the air indefinitely, whereas the largest particles fall in paths practically uninfluenced by the surrounding air flow. In this section the method of determining trajectories of aerial-spray droplets and the resulting distribution of deposit is presented.

Calculations of a similar nature have been performed by various investigators of aircraft icing problems. In these studies the trajectories of small water droplets moving in an airstream past various bodies such as airfoils and cylinders have been calculated to determine area and rate of droplet impingement on the surface. Glauert, in reference 2, considered cases wherein the air velocities and droplet diameters were sufficiently small ($R < 1$) so that the drag could be assumed proportional to the velocity of the droplet relative to the air (Stokes' law of resistance). Later, Langmuir and Blodgett (ref. 3) extended this work and considered the variation of drag beyond the limits of velocity and diameter

in which Stokes' law is valid. It was found, after a consideration of the range of droplet Reynolds numbers encompassed in aerial spraying, that the deviation of drag from Stokes' law should be included in the present calculations.

Equations of Motion

The motion of spray droplets in a space-fixed plane located behind the airplane perpendicular to the line of flight will be considered. A rectangular-coordinate system is used where vertical z distances are measured in airplane semispans from the ground plane (positive upward) and lateral y distances in semispans from the line of flight. If v_d and w_d are, respectively, the lateral and vertical components of droplet velocity and v_a and w_a the corresponding components of air velocity in the plane, the equations of motion which establish dynamic equilibrium of the forces acting on a droplet are

$$m \frac{dv_d}{dt} = D_y \tag{1}$$

$$m \frac{dw_d}{dt} = D_z - mg \tag{2}$$

The resultant aerodynamic drag force on the droplet is

$$D = \frac{1}{2} \rho_a \pi \left(\frac{\delta}{2}\right)^2 C_D \left[\left(v_a - v_d\right)^2 + \left(w_a - w_d\right)^2 \right]$$

and the lateral component of drag which appears in equation (1) may be expressed

$$D_y = D \frac{v_a - v_d}{\sqrt{\left(v_a - v_d\right)^2 + \left(w_a - w_d\right)^2}}$$

According to Stokes' law (see ref. 4, p. 598) the drag of spheres at very low Reynolds numbers ($R < 1$) is

$$D_{Stokes} = 6\pi\mu \frac{\delta}{2} \sqrt{(v_a - v_d)^2 + (w_a - w_d)^2}$$

Now, since

$$R = \frac{\rho_a \delta \sqrt{(v_a - v_d)^2 + (w_a - w_d)^2}}{\mu}$$

the ratio of the actual drag to the drag based on Stokes' law becomes

$$\frac{D}{D_{Stokes}} = \frac{C_D R}{24}$$

Since

$$m = \frac{4}{3} \pi \left(\frac{\delta}{2}\right)^3 \rho_d$$

$$R_U = \frac{\rho_a \delta U}{\mu}$$

and

$$\tau = \frac{Ut}{b}$$

the nondimensional equation of motion in the y-direction, after appropriate substitutions into equation (1), becomes

$$\frac{d(v_d/U)}{d\tau} = \frac{\sigma}{R_U} \frac{C_D R}{24} \left(\frac{v_a}{U} - \frac{v_d}{U}\right) \tag{3}$$

where

$$\sigma = 18 \frac{b}{\delta} \frac{\rho_a}{\rho_d}$$

In a similar manner the equation of motion in the z-direction (eq. (2)) becomes

$$\frac{d\left(w_d/U\right)}{d\tau} = \frac{\sigma}{R_U} \frac{C_D R}{24}\left(\frac{w_a}{U} - \frac{w_d}{U}\right) - \frac{bg}{U^2} \tag{4}$$

Except for the inclusion of the term due to gravity, bg/U^2, which appears in equation (4), equations (3) and (4) are of the same form as the equations of motion given in reference 3. Since the left-hand sides of equations (3) and (4) represent the accelerations of the droplet in the lateral and vertical directions, a double integration of these equations with prescribed initial values y_0, z_0, $\left(v_d/U\right)_0$, and $\left(w_d/U\right)_0$ defines the subsequent positions of the droplet.

In carrying out the integration of equations (1) and (2) it is necessary to evaluate R and $C_D R/24$ as the particle progresses along its trajectory. The Reynolds number of the droplet is computed from the relation

$$\left(\frac{R}{R_U}\right)^2 = \left(\frac{v_a}{U} - \frac{v_d}{U}\right)^2 + \left(\frac{w_a}{U} - \frac{w_d}{U}\right)^2 \tag{5}$$

and from reference 3 the term $C_D R/24$ is tabulated as a function of R in table I.

Air Velocities

The air velocities v_a and w_a as functions of droplet position and time are needed to solve equations (3) to (5). The two most significant disturbances behind an airplane are contributed by the wing and the propeller. Of these, the effect of propeller wash is largely localized to the vicinity behind the fuselage and its air disturbance velocities are approximately in the direction of the flight path. Because the

inclusion of these and other air velocities in the direction of flight would greatly complicate the analysis, and since such disturbances are believed to have a small effect on the lateral displacement of droplets, they have been neglected. The wing, on the other hand, sheds a sheet of vortices which soon roll up into two discrete vortex cores that are initially spaced somewhat less than a wing span apart. These so-called trailing vortices and the velocities induced by them in the yz-plane persist for a considerable time after the airplane's passage and appear to be of fundamental importance in determining the lateral distribution of droplets which impinge on the ground.

Idealized flow pattern.- An idealized flow pattern is used in the present analysis to approximate the velocities which are induced behind a wing. The trailing vortices and their images reflected from the ground plane are represented by a system of four parallel rectilinear vortices which pass perpendicularly through the yz-plane at points A, B, B', and A' (see fig. 1) and extend to infinity ahead of and behind this plane. The vortices are of equal strength and have the directions of rotation indicated by the figure. The coordinates of the vortex cores of this system change with time, since the coordinates of one of the vortex cores moves at the velocity induced at that point by the remaining three vortices. As a result, the trailing vortices are displaced downward and outward as depicted by the dashed lines in figure 1.

If the equations which express the velocities of the cores and the coordinates of their paths (ref. 4, pp. 223 to 224) are combined and integrated with respect to time, the positions of the cores as functions of time are obtained. If a rectangular spanwise loading is assumed, the strength of the trailing vortices is expressed as

$$\Gamma = \frac{C_L U b}{A}$$

and these relations then become

$$\tau = \frac{4\pi A}{C_L C_1}\left(-\frac{C_1\eta^2 - 2}{\sqrt{C_1\eta^2 - 1}} + C_2\right) \tag{6}$$

$$\tau = \frac{4\pi A}{C_L C_1}\left(\frac{C_1\zeta^2 - 2}{\sqrt{C_1\zeta^2 - 1}} + C_3\right) \tag{7}$$

where η and ζ are, respectively, lateral and vertical coordinates of the vortex core in semispans and the constants of integration are

$$C_1 = \frac{1}{\eta_0^2} + \frac{1}{\zeta_0^2}$$

$$C_2 = \frac{C_1\eta_0^2 - 2}{\sqrt{C_1\eta_0^2 - 1}}$$

$$C_3 = \frac{C_1\zeta_0^2 - 2}{\sqrt{C_1\zeta_0^2 - 1}}$$

The velocity components v_a/U and w_a/U induced by the vortex system at a point having coordinates y and z semispans are, by the Biot-Savart theorem,

$$\frac{v_a}{U} = \frac{C_L}{2\pi A}\left[\frac{\zeta + z}{(\zeta + z)^2 + (\eta - y)^2} - \frac{\zeta + z}{(\zeta + z)^2 + (\eta + y)^2} - \frac{\zeta - z}{(\zeta - z)^2 + (\eta + y)^2} + \frac{\zeta - z}{(\zeta - z)^2 + (\eta - y)^2}\right] \tag{8}$$

$$\frac{w_a}{U} = \frac{C_L}{2\pi A}\left[\frac{\eta - y}{(\zeta + z)^2 + (\eta - y)^2} + \frac{\eta + y}{(\zeta + z)^2 + (\eta + y)^2} - \frac{\eta + y}{(\zeta - z)^2 + (\eta + y)^2} - \frac{\eta - y}{(\zeta - z)^2 + (\eta - y)^2}\right] \tag{9}$$

The streamlines indicating the direction of air velocity vectors at a given time are shown in figure 2. The effect of foliage and other obstructions to air flow near the ground is, of course, neglected by the idealized flow pattern.

Because the induced velocities given by equations (8) and (9) become infinite at the position of the line vortices, it is necessary to consider the minimum radial distance from these points at which these equations remain applicable. In reference 5 an approximate expression is derived for the radius of the rolled-up vortex cores behind a wing. It is shown by simple energy considerations that the core radius for a wing having an elliptical spanwise loading is 0.155 semispan. In order to avoid the region of the vortex core, the spanwise starting positions of the droplets should be at least this distance from the center of the core.

Velocities in a real fluid.- Since the determination of velocities in the assumed flow field is based on an ideal fluid, it is of interest to consider briefly the effects of viscosity on the flow velocities in a real fluid, or, more specifically, the dissipation of vorticity with time.

To illustrate the effect of the decay of vorticity on the velocities induced in a real fluid, consider an isolated rectilinear vortex with an initial strength of Γ_0. At a subsequent time t, the circulation in a circle of radius r about the vortex (see ref. 4, p. 592) is

$$\Gamma = \Gamma_0\left(1 - e^{-r^2/4\nu t}\right) \tag{10}$$

Hence the tangential velocity on the circle becomes

$$q_{viscous} = \frac{\Gamma}{2\pi r}\left(1 - e^{-r^2/4\nu t}\right) \tag{11}$$

and therefore

$$\frac{q_{viscous}}{q_{ideal}} = \left(1 - e^{-r^2/4\nu t}\right) \tag{12}$$

Equation (12) is plotted against r for various values of time in figure 3. The figure shows the extremely slow rate at which induced velocities a few feet from the vortex line are diminished as a result of viscosity.

An additional viscous effect not accounted for by the idealized flow pattern is evidenced in the form of a boundary layer of reduced air velocities adjacent to the ground.

Trajectory Computations

The sample airplane for which the trajectory computations were made is the Ag-1, a single-engine, low-wing, agricultural airplane of moderate size. The liquid droplets are assumed to have the density of kerosene, a frequently used solvent for insecticides. The physical characteristics pertinent to these computations are given in table II.

A step-by-step integration of equations (1) and (2) was accomplished on the Bell Telephone Laboratories X-66744 relay computer at the Langley Laboratory. It was found convenient to tabulate the variation of $C_D R/24$ with R for several values of R and use a linear interpolation between the tabulated values. The coordinates of the trailing vortex cores were determined in a similar manner by tabulating η and ζ at suitably chosen values of τ. The air velocities were computed at each point along the trajectory by evaluating equations (8) and (9) directly.

A series of trajectories was computed for several flight conditions with selected values of the parameters σ and R_U and with assigned initial conditions y_0, z_0, $\left(v_d/U\right)_0$, and $\left(w_d/U\right)_0$. In order to reduce the number of computed points along a trajectory and yet retain a reasonable degree of accuracy, the time increments during an integration were varied; the criterion used to select these time intervals was the change in the droplet acceleration evaluated at two adjacent points. The integration was stopped when the particle intersected the ground plane or when its trajectory looped about the vortex core.

The vortex cores are assumed initially to be at the height of the airplane and separated laterally a distance of 1 span. Particles are given starting positions at various points along a line connecting the trailing vortices, and the initial droplet velocity is taken to be the steady-state velocity of the droplet if it were falling under the influence of gravity in a uniform airstream having velocity components equal to the induced velocities of the idealized flow pattern at the point of release. This assumption was made, rather than the assumption that the particles were released from rest at the trailing edge, in order to compensate somewhat for the error caused by neglecting the bound vortex in regions close to the wing (see appendix A). Actually, in the neighborhood of the wing, air velocities are induced by a bound vortex at the wing and, in addition, a continuous sheet of vorticity extending downstream from the bound vortex. In the present case, where a simplified uniform spanwise loading is considered, the flow in this region may be

represented by a single horseshoe-vortex arrangement with a bound vortex at the quarter-chord point connected with trailing vortices of equal strength which terminate at the wing tip and extend downstream to infinity. By neglecting the bound vortex, the initial downwash is underestimated, although this error in downwash is to some extent reduced by the forward-extending vortices assumed in the idealized flow pattern.

At a distance of 2.0 semispans behind the bound vortex the velocities induced by the idealized flow pattern were found to be within 6 percent of the velocities induced by the horseshoe-vortex system. The approximate error in the vertical position of a droplet 2.0 semispans downstream of the wing, caused by an underestimation of the downwash ahead of this point together with the compensating assumption of a finite downward ejection velocity, is evaluated in appendix A.

A summary of the results of droplet-trajectory computations is given in table III. Here, the quantities y_0, y_g, v_{d_g}, w_{d_g}, and t_g are given for the various droplet sizes and airplane flight conditions considered in the analysis. The calculated droplet trajectories for these cases are plotted in figure 4.

Distribution of Deposit

From the foregoing trajectory computation it is possible to determine the distribution of deposit for various assumed nozzle characteristics and spanwise rates of efflux. Consider first the case where a spray, composed of particles of various sizes, is introduced into the flow field at point (y_0, z_0) and at the rate of Q pounds per unit length along the flight path. For each droplet size there is a corresponding position of impingement on the ground y_g; therefore, droplets of size δ and $\delta + \Delta\delta$ fall at y_g and $y_g + \Delta y_g$, respectively. The rate at which mass is deposited in element Δy_g is $Q\,\Delta v$ where Δv is the percentage of Q which is represented by droplets having diameters between δ and $\delta + \Delta\delta$. The concentration of deposit at position y_g is then

$$C = Q \frac{\Delta v}{\Delta y_g} \tag{13}$$

which, in the limit, can be written

$$C = Q \frac{dv}{d\delta} \frac{d\delta}{dy_g} \tag{14}$$

Equation (14) applies for a single nozzle, and by superposition the concentration of deposit can be determined for any number of nozzles. For a large number of nozzles closely spaced along the wing, however, it is more convenient to consider mass as being ejected continuously along the span rather than at a finite number of discrete points.

The rate of change of concentration at y_g with respect to Q is, by equation (14),

$$\frac{dC}{dQ} = \frac{dv}{d\delta}\frac{d\delta}{dy_g} \tag{15}$$

but, since Q is a continuous function of y_0,

$$dQ = \frac{dQ}{dy_0}\,dy_0$$

Therefore, the total concentration at y_g due to a continuous mass flow along the span becomes

$$C = \int_0^{y_0} \frac{dQ}{dy_0}\frac{dv}{d\delta}\frac{d\delta}{dy_g}\,dy_0 \tag{16}$$

In order to compute the concentration of deposit by means of equation (14) or (16), suitable expressions for the terms $dv/d\delta$ and $d\delta/dy_g$ must be determined. The relation $dv/d\delta$ is defined by the nozzle or spray characteristics, and $d\delta/dy_g$ is associated with the trajectories of droplets.

Nozzle and Spray Characteristics

Reference 6 shows that the breakup of liquid jets, ejected into a high-velocity airstream, is dependent on the Reynolds number of the mean droplet size and the relative viscosities of the liquid particles and the surrounding air. The nozzle bore was found to have no effect on the mean droplet size except at very low ejection velocities, in which case the droplets were more uniform and had diameters approximately twice that of the nozzle.

An empirical expression for the mean diameter, which is applicable for all conditions likely to be encountered in aerial spraying, is given in reference 6. In the notation of the present paper the expression is

$$\delta_m = \frac{500\nu_d^{1/5}}{V} \tag{17}$$

where the mean diameter δ_m is the droplet size in cm about which the largest percentage of the total volume is concentrated, V is the relative velocity in cm/sec between the liquid jet and the air, and ν_d is the kinematic viscosity of the liquid in cm^2/sec.

The spectra of droplet sizes measured in reference 6 were symmetrical, so the droplet size at 50 percent volume was taken to be δ_m. Moreover, the measured distribution of droplet sizes appeared to have the form of the so-called normal distribution found in the theory of probability. The equation of the normal distribution (see ref. 7) then provides the following mathematical expression for the term $dv/d\delta$ appearing in equations (14) and (16):

$$\frac{dv}{d\delta} = \frac{0.675}{\epsilon\sqrt{2\pi}} e^{-1/2\left[\frac{0.675(\delta - \delta_m)}{\epsilon}\right]^2} \tag{18}$$

The term ϵ in equation (18) is known as the "probable error" and in the present problem represents the dispersion or spread of droplet sizes about δ_m; that is, ϵ is such that 50 percent of the volume is composed of droplets having diameters between $\delta_m - \epsilon$ and $\delta_m + \epsilon$. The magnitude of ϵ is then a measure of the uniformity of droplet sizes in a liquid spray having a mean diameter δ_m.

Two sample spectra of droplet sizes are considered in the present analysis; these have mean diameters of 200 and 300 microns and a dispersion ϵ of 50 microns. The percentage of the total mass in terms of droplet diameter may be determined by integrating equation (18), a plot of which is given in figure 5 for the two droplet spectra under consideration. (See tabulated values of the probability integral in ref. 8.)

Mathematical Representation of Trajectory Data

An empirical relation which expresses the droplet diameter as a function of y_0 and y_g for a given flight condition is derived in appendix B by applying the method of least squares to the trajectory data presented in table III. An equation which was found to give a satisfactory approximation of the computed data is

$$\delta = k_1 + k_2 P + k_3 P^2 \tag{19}$$

where

$$P = \frac{1}{y_g - y_0}$$

and the coefficients k_1, k_2, and k_3 are functions of y_0. It is seen that equation (19) satisfies the condition that the droplets which descend in practically vertical paths $\left(y_g \approx y_0\right)$ are very large, whereas the droplets which are carried away in the vortex flow $\left(y_1 \rightarrow \infty\right)$ have finite diameters equal to or smaller than k_1.

Figure 4 indicates that as the droplet diameter is reduced the influence of disturbance velocities becomes more pronounced, until finally a critical condition is reached wherein the path of the droplet encircles the vortex core. It appears from the limited number of trajectory computations available that once the particle encircles a vortex core it continues to do so for a considerable time, during which it is carried laterally outward with the trailing-vortex core. Eventually the induced velocities become dissipated sufficiently so that they can no longer sustain the particle and it falls to the ground; however, the mass represented by such particles and also the mass "lost" through evaporation is neglected in determining the concentration of deposit.

To determine the percentage of mass carried away by the vortex velocities it is necessary to consider the droplet spectrum and the spanwise position from which droplets were ejected. Since coefficient k_1 in equation (19) represents the minimum droplet diameter which is recovered, in terms of the starting position, the percentage of mass neglected by the analysis is simply the percent volume corresponding to $\delta = k_1$ in figure 5. In figure 6, the ratio of the mass recovered to the total mass

ejected is plotted as a function of the droplet starting position for the two sample droplet-size spectra with $C_L = 1.2$ and $z_0 = 0.5$ semispan. When adjacent swaths are overlapped in order to cover a given area more uniformly, the part of the mass which is neglected by the analysis, but does not evaporate, is probably distributed more or less uniformly over the entire area.

RESULTS AND DISCUSSION

Distribution of Deposit With Discrete Nozzles

When liquid is ejected behind the wing from a discrete point, such as a nozzle, the resulting concentration of deposit on the ground may be determined by evaluating equation (14) with the aid of equations (18) and (19) at various y_g positions on the ground. The distribution of deposit so computed is presented in figures 7 to 9 for a unit mass efflux rate. These figures are intended to illustrate the effect of spanwise location of the nozzle, mean diameter of the droplets, airplane lift coefficient, and airplane height.

The effect of the mean diameter of the droplets on the shape of the deposit curves is shown in figure 7 for the case of $C_L = 1.2$ and $z_0 = 0.5$ semispan. Here, the deposit curves are characterized by high peaks of concentration when the nozzles are located near the plane of symmetry $\left(y_0 = 0.25 \text{ semispan}\right)$, whereas for nozzle locations in the vicinity of the wing tip $\left(y_0 = 0.75 \text{ semispan}\right)$ the concentration of deposit is less intense and the distribution is more uniform. This effect would be expected since the magnitude and curvature of the air-flow velocities are increased as the wing tip is approached, and, as a consequence, droplets of different diameters are dispersed more in this region than at points farther inboard.

Curves for various values of mean diameter of the droplets indicate that as δ_m is reduced the deposit is distributed over a larger area, the center of which is displaced slightly farther outboard.

The effect of airplane lift coefficient on the deposit curves is illustrated in figure 8, where the altitude is again taken to be 0.5 semispan and $\delta_m = 300$ microns. At $C_L = 2.2$, the lift coefficient corresponding to the flaps-down condition, the deposit curve is of similar shape but displaced farther outboard than for the flaps-up case $\left(C_L = 1.2\right)$. It is of interest to note that the velocity of impingement for the flaps-down case (see table III) is generally slightly higher than for the corresponding flaps-up case. The higher droplet velocities and also the stronger

air-disturbance velocities which accompany the use of flaps may provide greater penetration of the crop foliage by the sprayed liquid.

A comparison of the deposit curves calculated for flight altitudes of 0.5 and 1.0 semispan is shown in figure 9, where $C_L = 1.2$ and $\delta_m = 300$ microns. The figure indicates that the uniformity and lateral displacement of the deposit is increased with airplane altitude.

Distribution of Deposit With Continuous Spanwise Mass Flow

In practice, aerial sprays are generally issued from many nozzles along the span. In order to calculate the total concentration of deposit when there is a multitude of closely spaced nozzles, it is convenient to use equation (16), which is the integral form of equation (14). Variations of dQ/dy_0 were assumed and the resulting concentrations of deposit were determined by integrating equation (16) numerically with the use of Simpson's rule. In performing these computations the available trajectory data (table III) were extrapolated by means of equation (19) so as to encompass a range of spanwise starting positions from $y_0 = 0$ to $y_0 = 0.8$ semispans. In the results which follow, $C_L = 1.2$, $z_0 = 0.5$ semispan, and the mass efflux rate is assumed to be zero beyond $y_0 = 0.8$ semispan.

In figure 10 are presented deposit curves evaluated for a uniform spanwise efflux rate (solid lines in the figure) and also deposit curves in which dQ/dy_0 was modified in an attempt to improve the uniformity of deposit (dashed lines). For the case of a uniform spanwise mass efflux rate the deposit curves for both of the droplet-size spectra considered show maximum concentration at the plane of symmetry. The deposit curve for $\delta_m = 300$ microns (fig. 10(b)) is the less uniform of the two; it has a higher concentration at the plane of symmetry but at $y_g = 2.0$ semispans it has about one-half the concentration of the deposit curve for $\delta_m = 200$ microns (fig. 10(c)). The deposit is, of course, reduced to zero in all cases as y_g becomes large.

For the purpose of determining a modified spanwise efflux rate which would improve the uniformity of deposit, assume that all of the droplets issued from the wing were of equal size (δ = Constant). Each of the droplets ejected at a point y_0 would then fall at a single point y_g on the ground in accordance with the trajectory characteristics of the droplet size in question. The concentration of deposit in this case would be

$$C = \frac{dQ}{dy_0}\frac{dy_0}{dy_g} \tag{20}$$

Therefore, the variation of dQ/dy_0 with y_0 required to provide a uniform deposit of a constant-droplet-size spray becomes

$$\frac{dQ}{dy_0} = \frac{\text{Constant}}{dy_0/dy_g} \tag{21}$$

where dy_0/dy_g is expressed as a function of y_0 alone by the simultaneous solution of equation (19), with δ equal to a constant, and the relation

$$\frac{dy_0}{dy_g} = -\frac{\partial\delta/\partial y_g}{\partial\delta/\partial y_0} \tag{22}$$

Although this procedure for determining the optimum spanwise variation of mass flow rate is true only for sprays of constant droplet size, the uniformity of deposits having a variable droplet size should be improved by varying the mass flow rate in accordance with equation (21), taking the droplet size to be the mean diameter of the droplets.

The modified efflux rate I in figure 10(a) is equation (21) evaluated with δ = 300 microns. The constant in equation (21) was selected to give the same total mass flow per unit length along the flight path as was assume for the case of a constant spanwise flow rate (Q = 0.8 pound per unit length The resulting deposit is shown by the appropriate coded curve in figure 10(b Here, the peak deposit which occurs at y_g = 1.1 semispans indicates that too large a portion of the mass is transported laterally outward. One method of overcoming this difficulty would be to evaluate equation (21) for a droplet diameter somewhat larger than δ_m.

The mass flow rate evaluated to give a uniform deposit with a constant-diameter spray of 350 microns is denoted by II in figure 10(a). The corresponding deposit for the case of a spectrum of 300-micron mean diameter is shown in figure 10(b). Here, the distribution of deposit is seen to be approximately uniform up to y_g = 1.2 semispans, and beyond this point it breaks off abruptly as do the other deposit curves in figure 10(b); however, the lateral extent of the deposits of variable mass flow rate is somewhat greater than the deposit calculated for a uniform mass flow rate.

Since a more favorable deposit results when the diameter used to evaluate equation (21) is somewhat larger than the mean diameter of the droplet spectrum, efflux rate I was used to modify the deposit curve for

δ_m = 200 microns. The resulting deposit is shown in figure 10(c). The concentration of the modified deposit for δ_m = 200 microns is less intense but is uniform over a larger region than the modified deposit with δ_m = 300 microns. Moreover, there is no abrupt reduction in the intensity of concentration beyond y_g = 1.2 semispans as was the case for δ_m = 300 microns.

In addition to varying the mass flow rate along the wing, there remains the possibility of regulating the mean diameter of the droplet spectrum at various nozzle locations along the wing. As indicated in equation (17), this could be accomplished through control of the relative jet velocity, which is dependent on the direction of the jet relative to the surrounding airstream and the pressure under which liquid is ejected.

To investigate one such case, it was assumed that the mean diameter increased linearly from 200 microns at the plane of symmetry to 300 microns at y_0 = 0.8 semispan and that the spanwise efflux rate was held constant. In this example, the spectrum of smallest mean diameter (δ = 200 microns) was issued from the plane of symmetry in order to reduce the peak deposit which occurred in this region when sprays of similar spectra were issued at a uniform rate across the span. The distribution of deposit for this case is plotted in figure 11. It is seen that this deposit curve has characteristics similar to the modified deposit of figure 10(b), where the uniformity of deposit was improved by increasing the mass flow rate with distance from the midspan.

Effect of Flight-Path Spacing on Distribution of Deposit

Thus far, an attempt has been made to improve the uniformity of the lateral deposit of an isolated swath. In actual practice, however, uniformity of the deposit is dependent upon not only the distribution of concentration within a single swath, but also the manner in which the swaths are superimposed, that is, the lateral spacing of adjacent passes of the airplane.

Since flight-path spacing is an important factor with regard to economy of operation, its effect on the total distribution of deposit has been determined for several of the individual swaths shown in figure 10. These results are presented in figure 12. In order to determine the total concentration of deposit, the ordinates of overlapping swaths are added as illustrated in figure 12(a). If an optimum deposit is taken to be one in which the minimum required concentration is distributed uniformly on the ground, the concentration which exceeds this required minimum value will constitute an excess of deposit. A ratio of the excess deposit (hatched area in fig. 12(a)) to the total deposit may therefore

be considered a measure of the uniformity of the swath. The variation of this ratio with lateral flight-path spacing is plotted in figure 12(b) for δ_m = 300 microns and in figure 12(c) for δ_m = 200 microns. The coded lines correspond to the efflux rates given by figure 10(a).

These plots indicate that for a similar degree of uniformity in the swath, the flight-path spacing can be increased by modifying the efflux rate in the manner shown in figure 10(a). For example, if 10 percent excess deposit is considered tolerable, the modified flow rate would permit an increase in the flight-path spacing of approximately 0.4 semispan for δ_m = 300 microns and 1.0 semispans for δ_m = 200 microns. A second conclusion to be drawn from figure 12 is that, of the two spray spectra considered, the spray with δ_m = 200 microns provides a more uniform swath for equivalent flight-path spacings. Furthermore, the uniformity of this swath appears to be somewhat less sensitive to flight-path spacing. This consideration would be of importance in cases where it is difficult to estimate the optimum spacing between adjacent passes of the airplane.

CONCLUSIONS

Results of the foregoing analysis of factors affecting the dispersion of spray droplets issued from a moderate-size agricultural airplane indicate that:

1. Greater lateral dispersion of aerial sprays will result when the position at which droplets are ejected is moved toward the wing tip, when the mean diameter of the droplet spectrum is reduced, or when either the airplane lift coefficient or the altitude is increased.

2. The uniformity and effective width of the swath is improved by increasing the mass efflux rate with distance from the midspan.

3. As compared with a spray spectrum of 300-micron mean diameter, the spray spectrum with a mean diameter of 200 microns allows greater flight-path spacing and produces a more uniform deposit. Moreover, the degree of uniformity is less sensitive to changes in the spacing of adjacent passes of the airplane.

Langley Aeronautical Laboratory,
National Advisory Committee for Aeronautics,
Langley Field, Va., August 4, 1953.

APPENDIX A

EVALUATION OF ERROR IN DROPLET POSITION DUE TO PROXIMITY OF THE BOUND VORTEX

When a particle is released from the trailing edge of a wing, the velocity induced by the bound vortex may represent a substantial part of the total velocity acting on the particle during the initial part of its motion. In the present analysis an attempt to account for this additional downwash was made by simply assuming that particles were ejected downward from the trailing edge. The initial velocities of the particles were assumed to be equal to their steady velocities when falling through a uniform stream having an air velocity equivalent to the velocity induced by the idealized flow pattern at the initial position of the droplet. In this appendix, the errors introduced by such an assumption are evaluated for the case in which the wing is represented by a horseshoe vortex.

In computing these errors it is convenient to determine an air-velocity correction which, when added to the idealized flow velocities, will provide the velocities induced by a horseshoe-vortex system. The required correction is seen to be the velocity induced by a horseshoe vortex of span 2b with legs extending forward to infinity in the direction of flight. The strength of this horseshoe vortex is the same as the strength of the vortices in the idealized flow field and its sense of rotation is such that, when superimposed upon the idealized vortex arrangement, the forward-extending legs cancel the vortices which would otherwise extend to infinity ahead of the airplane. The correction velocity induced by the horseshoe vortex reflected from the ground plane is small in relation to the velocity induced by the bound vortex at the wing and in the present approximation will be neglected.

For convenience the origin of coordinates in this case is taken at the center of the bound vortex with x positive in a rearward direction and z' positive in an upward direction. The downwash-velocity correction (denoted by the subscript c) in the xy-plane is given by the relation

$$\left(\frac{w_a}{U}\right)_c = -\frac{C_L}{4\pi A}\left\{\frac{1}{x}\left[\frac{\sqrt{(1-y)^2+x^2}}{1-y}+\frac{\sqrt{(1+y)^2+x^2}}{1+y}\right]-\frac{2}{(1-y)(1+y)}\right\} \tag{A1}$$

At $x = 2.0$ semispans, the velocity on the midspan given by equation (A1) is approximately 5.8 percent of the downwash induced by the idealized flow field when $\tau = 0$ and the airplane altitude is 0.5 semispan. Consequently, the error in droplet position associated with the error in induced downwash beyond $x = 2.0$ semispans will be assumed to be negligible. Moreover, it will also be assumed in the following calculations that the vortex cores are held fixed during the time required for the airplane to travel 2.0 semispans, and that the downwash-velocity correction does not change with the departure of the droplet from the xy-plane. The last two assumptions lead to overestimation of the magnitude of the downwash correction whereas the first leads to underestimation of its duration.

If the equation for vertical motion of a droplet (eq. (2)) in the idealized flow field is subtracted from a similar equation in which the downwash-velocity correction (eq. (A1)) and the increment in drop velocity due to this downwash correction have been included, the resulting equation when $C_DR/24$ is constant is

$$\frac{d\left(\frac{w_d}{U}\right)_c}{d\tau} = \frac{\sigma}{R_U}\frac{C_DR}{24}\left[\left(\frac{w_a}{U}\right)_c - \left(\frac{w_d}{U}\right)_c\right] \tag{A2}$$

which may be written

$$\frac{d^2z'_c}{d\tau^2} + \frac{\sigma C_DR}{R_U 24}\frac{dz'_c}{d\tau} = \frac{\sigma C_DR}{R_U 24}\left(\frac{w_a}{U}\right)_c \tag{A3}$$

An integration of equation (A3) over a distance extending from the trailing edge of the wing ($x = 0.3$ semispan) to a position 2.0 semispans downstream of the bound vortex gives the approximate vertical droplet-position error caused by using the idealized flow pattern rather than a horseshoe vortex in the neighborhood of the wing. If the horizontal droplet position (in semispans) downstream of the bound vortex is given by $\frac{Ut}{b} + 0.3$, where U is the airplane flight speed, the additional downwash $\left(w_a/U\right)_c$ acting on a droplet released from the trailing edge may be determined by substituting $\tau = x - 0.3$ into equation (A1), where $\tau = \frac{Ut}{b}$. It was found that over the interval $0.3 \leqq x \leqq 2.0$ semispans and for y values equal to or less than 0.75 semispan, equation (A1) was essentially independent of spanwise distance y. An empirical relation

which gives a satisfactory approximation of equation (A1) over this interval is

$$\frac{4\pi A}{C_L}\left(\frac{w_a}{U}\right)_c = -4.09 + 6.60\tau - 2.62\tau^2 \qquad (A4)$$

where $0 \leqq \tau \leqq 1.7$

The drag term $C_D R/24$ of a droplet falling at a steady-state condition in a uniform stream is the same as if the droplet were falling at its terminal velocity through still air. Therefore, equation (4) for a steady condition reduces to

$$-\left(\frac{w_d}{U}\right)_t \frac{C_D R_t}{24} = \frac{R_U}{\sigma}\frac{bg}{U^2} \qquad (A5)$$

where the subscript t denotes a terminal velocity condition and this velocity is in a negative direction. Equation (A5) may be written in a more convenient form as

$$-R_t \frac{C_D R_t}{24} = \frac{R_U^2}{\sigma}\frac{bg}{U^2} \qquad (A6)$$

which, together with the functional relation between $C_D R/24$ and R (table I), defines $C_D R_t/24$, the constant coefficient in equation (A3).

Equation (A3) may now be put into the form

$$\frac{d^2 z'_c}{d\tau^2} + \alpha \frac{dz'_c}{d\tau} = \alpha\left(a_0 + a_1\tau + a_2\tau^2\right) \qquad (A7)$$

where

$$\alpha = \frac{\sigma}{R_U}\frac{C_D R_t}{24}$$

The general solution of equation (A7) is

$$z'_c = C_1 e^{-\alpha\tau} + \left(a_0 - \frac{a_1}{\alpha} + \frac{2a_2}{\alpha^2}\right)\tau + \left(a_1 - \frac{2a_2}{\alpha}\right)\tau^2 + a_2\tau^3 + C_2 \qquad \text{(A8)}$$

With the initial conditions

$$\tau = 0$$

$$z'_c = \frac{dz'_c}{d\tau} = 0$$

the arbitrary constants become

$$C_1 = -C_2 = \frac{a_0}{\alpha} - \frac{a_1}{\alpha^2} + \frac{2a_2}{\alpha^3} \qquad \text{(A9)}$$

When equation (A8), with constants defined by equation (A9), is evaluated at $\tau = 1.7$, the value obtained is the approximate error in vertical droplet position caused by using the idealized flow rather than the flow induced by a horseshoe vortex. The downwash is underestimated when the idealized flow field is used, so the correction is additive in a downward direction.

It remains to determine the influence of the assumption used to compensate approximately for neglect of the bound vortex, namely, that droplets are ejected at a finite downward velocity

$$\left(\frac{w_d}{U}\right)_{\tau=0} = \frac{w_a}{U} + \left(\frac{w_d}{U}\right)_t \qquad \text{(A10)}$$

Let $\Delta z'$ be the total difference in distance traveled by a particle ejected into an airstream at a finite velocity (eq. (A10)) and a similar particle released from rest into the same airstream. If the airstream is considered to have a uniform velocity w_a/U and the drag term $C_D R_t/24$

is again taken to be constant, $\Delta z'$ (in semispans) from the differential equation of droplet motion becomes

$$\Delta z' = \frac{\frac{w_a}{U} + \left(\frac{w_d}{U}\right)_t}{\alpha} \qquad \text{(A11)}$$

The approximate total error in vertical droplet position which may be expected as a result of the assumed starting conditions used in the trajectory computations is then the difference between equations (A8) and (A11). This error was evaluated at several spanwise starting positions for the flight conditions $C_L = 1.2$ and $z_0 = 0.5$ semispan and for droplet diameters of 200 and 300 microns (the mean diameters of spray spectra to be considered).

The calculated errors in vertical droplet position (in semispans) for these conditions are as follows:

y_0, semispans	Error* (semispans) for -	
	δ = 200 microns	δ = 300 microns
0.25	-0.017	0.004
.50	-.011	.013
.75	.005	.053

*A negative sign indicates that the error is in an upward direction.

Similar computations were made for the error in lateral droplet position caused by neglect of the horseshoe vortex. The corrected lateral droplet position was inboard of the calculated position; however, the magnitude of the correction was found to be insignificant.

APPENDIX B

LEAST-SQUARES REPRESENTATION OF TRAJECTORY DATA

In the computation of the distribution of deposit for the case of a discrete nozzle the unknown coefficients k_1, k_2, and k_3 and the spanwise starting position y_0 in equation (19) are constant. It is desired to determine the values of k_1, k_2, and k_3 in the formula

$$\delta = k_1 + k_2 P + k_3 P^2 \tag{B1}$$

which give the best approximation of n data points (table III) at the particular y_0 value in question. The principle of least squares provides a method of computing these coefficients which minimizes the sum of the squares of the differences between the values of δ in table III and the values of δ computed from equation (B1). Thus the three unknown coefficients may be determined by solving the following set of simultaneous equations:

$$\left.\begin{aligned} \sum \delta &= k_1 n + k_2 \sum P + k_3 \sum P^2 \\ \sum P\delta &= k_1 \sum P + k_2 \sum P^2 + k_3 \sum P^3 \\ \sum P^2\delta &= k_1 \sum P^2 + k_2 \sum P^3 + k_3 \sum P^4 \end{aligned}\right\} \tag{B2}$$

The deposit for discrete nozzles was evaluated only at the y_0 positions for which trajectory computations were available. This limitation obviated the necessity of interpolating to determine the coefficients at other y_0 positions; however, in determining the deposit for the case of a continuous spanwise distribution of mass flow (eq. (16)), the variations of k_1, k_2, and k_3 with y_0 must be known. From experience gained while determining the coefficients of equation (B2) for various values of y_0, it was found that the variation of these coefficients with y_0 could be satisfactorily approximated by the relations

$$\left.\begin{aligned} k_1 &= a_2 y_0^2 + a_3 y_0^3 \\ k_2 &= b_1 y_0 + b_2 y_0^2 \\ k_3 &= c_1 y_0 + c_2 y_0^2 \end{aligned}\right\} \tag{B3}$$

Equation (B1) then becomes

$$\delta = a_2 y_0^2 + a_3 y_0^3 + b_1 y_0 P + b_2 y_0^2 P + c_1 y_0 P^2 + c_2 y_0^2 P^2 \qquad (B4)$$

Equation (B4) contains six unknown coefficients, and for the case in which $C_L = 1.2$ and $z_0 = 0.5$ semispan (the flight condition for which the deposit with a continuous mass flow was evaluated) there is a total of 20 data points (see table III). Applying the method of least squares to equation (B4) provides a set of six simultaneous equations:

$$\sum y_0^2 \delta = a_2 \sum y_0^4 + a_3 \sum y_0^5 + b_1 \sum P y_0^3 + b_2 \sum P y_0^4 + c_1 \sum P^2 y_0^3 + c_2 \sum P^2 y_0^4$$

$$\sum y_0^3 \delta = a_2 \sum y_0^5 + a_3 \sum y_0^6 + b_1 \sum P y_0^4 + b_2 \sum P y_0^5 + c_1 \sum P^2 y_0^4 + c_2 \sum P^2 y_0^5$$

$$\sum P y_0 \delta = a_2 \sum P y_0^3 + a_3 \sum P y_0^4 + b_1 \sum P^2 y_0^2 + b_2 \sum P^2 y_0^3 + c_1 \sum P^3 y_0^2 + c_2 \sum P^3 y_0^3$$

$$\sum P y_0^2 \delta = a_2 \sum P y_0^4 + a_3 \sum P y_0^5 + b_1 \sum P^2 y_0^3 + b_2 \sum P^2 y_0^4 + c_1 \sum P^3 y_0^3 + c_2 \sum P^3 y_0^4$$

$$\sum P^2 y_0 \delta = a_2 \sum P^2 y_0^3 + a_3 \sum P^2 y_0^4 + b_1 \sum P^3 y_0^2 + b_2 \sum P^3 y_0^3 + c_1 \sum P^4 y_0^2 + c_2 \sum P^4 y_0^3$$

$$\sum P^2 y_0^2 \delta = a_2 \sum P^2 y_0^4 + a_3 \sum P^2 y_0^5 + b_1 \sum P^3 y_0^3 + b_2 \sum P^3 y_0^4 +$$

$$c_1 \sum P^4 y_0^3 + c_2 \sum P^4 y_0^4$$

These equations may be solved for the unknown coefficients (a_2, a_3, and so forth) by any convenient method of solving linear simultaneous algebraic equations.

The following numerical values of the coefficients in equation (B4) were determined for the case in which $C_L = 1.2$ and $z_0 = 0.5$ semispan:

$$a_2 = 373.7$$

$$a_3 = -157.4$$

$$b_1 = 216.9$$

$$b_2 = -49.76$$

$$c_1 = -0.0537$$

$$c_2 = -8.141$$

The comparison of the points determined by trajectory computations and the empirical representation of these points by equation (B4) is shown in figure 13.

REFERENCES

1. Yuill, J. S., Davis, R. H., et al.: Studies of the Factors Affecting the Distribution and Deposit of Aerial Sprays. Progress Report, 1948 Season, Forest Insect Laboratory (Beltsville, Md.), Mar. 24, 1949.

2. Glauert, Muriel: A Method of Constructing the Paths of Raindrops of Different Diameters Moving in the Neighbourhood of (1) a Circular Cylinder, (2) an Aerofoil, Placed in a Uniform Stream of Air; and a Determination of the Rate of Deposit of the Drops on the Surface and the Percentage of Drops Caught. R. & M. No. 2025, British A.R.C., Nov. 10, 1940.

3. Langmuir, Irving, and Blodgett, Katherine B.: A Mathematical Investigation of Water Droplet Trajectories. AAF TR No. 5418 (Contract No. W-33-038-ac-9151), Air Technical Service Command, Army Air Forces, Feb. 19, 1946.

4. Lamb, Horace: Hydrodynamics. Reprint of sixth ed. (first American ed.), Dover Publications, 1945.

5. Spreiter, John R., and Sacks, Alvin H.: The Rolling Up of the Trailing Vortex Sheet and Its Effect on the Downwash Behind Wings. Jour. Aero Sci., vol. 18, no. 1, Jan. 1951, pp. 21-32, 72.

6. Merrington, A. C., and Richardson, E. G.: The Break-Up of Liquid Jets. Proc. Physical Soc. (London), vol. 59, pt. 1, no. 331, Jan. 1, 1947, pp. 1-13.

7. Forsyth, C. H.: An Introduction to the Mathematical Analysis of Statistics. John Wiley & Sons, Inc., 1924.

8. Peirce, B. O.: A Short Table of Integrals. Third rev. ed., Ginn and Co., 1929.

TABLE I.- VALUES OF $C_DR/24$ AS A FUNCTION OF R*

R	$C_DR/24$	R	$C_DR/24$
0	1.00	14.0	2.009
.05	1.009	16.0	2.109
.1	1.018	18.0	2.198
.2	1.037	20.0	2.291
.4	1.073	25.0	2.489
.6	1.103	30.0	2.673
.8	1.142	35.0	2.851
1.0	1.176	40.0	3.013
1.2	1.201	50.0	3.327
1.4	1.225	60.0	3.60
1.6	1.248	80.0	4.11
1.8	1.267	100.0	4.59
2.0	1.285	120.0	5.01
2.5	1.332	140.0	5.40
3.0	1.374	160.0	5.76
3.5	1.412	180.0	6.16
4.0	1.447	200.0	6.52
5.0	1.513	250.0	7.38
6.0	1.572	300.0	8.26
8.0	1.678	350.0	9.00
10.0	1.782	400.0	9.82
12.0	1.901	500.0	11.46

*From reference 3.

TABLE II.- AIRPLANE AND SPRAY CHARACTERISTICS

Wing semispan, b, ft	19.5
Wing aspect ratio, A	5.35
Density of droplets, ρ_d, slugs/cu ft	1.55
Density of air, ρ_a, slugs/cu ft	0.002375
Lift coefficient of airplane, C_L	1.2; 2.0
Flight velocity, U, ft/sec	85.0;62.6

TABLE III.- TABULATED RESULTS OF DROPLET-TRAJECTORY DATA

(a) $C_L = 1.2$; $z_0 = 0.5$ semispan

y_0, semispans	y_g, semispans (*)	δ, microns	v_{d_g}, ft/sec	w_{d_g}, ft/sec	t_g, sec
0.25	0.506	210	2.09	-1.97	2.88
.25	.441	275	2.08	-3.08	2.26
.25	.385	375	2.06	-4.21	1.71
.25	.347	500	2.01	-5.65	1.31
.25	.313	700	1.83	-8.75	.95
.50	1.675	150	10.38	-1.11	3.03
.50	1.130	210	9.95	-2.12	2.18
.50	.925	275	7.84	-3.03	1.77
.50	.795	375	6.45	-4.40	1.42
.50	.710	500	5.13	-6.83	1.15
.50	.628	700	4.66	-9.16	.84
.625	(**)	150	-----	-----	----
.625	1.670	210	8.76	-1.67	2.42
.625	1.250	275	11.47	-2.91	1.61
.625	1.006	375	10.03	-4.44	1.35
.625	.893	500	8.93	-5.71	1.00
.625	.787	700	6.77	-9.51	.75
.75	(**)	210	-----	-----	----
.75	1.77	275	6.56	-2.56	2.26
.75	1.33	375	11.03	-3.84	1.25
.75	1.10	500	11.01	-6.02	.95
.75	.95	700	8.82	-9.66	.65

*The y_g values are without cross wind. To account for a cross wind, the product of t_g and the cross-wind velocity component may be applied as a correction to the tabulated y_g values.

**Computations were discontinued before droplet intersected ground plane.

TABLE III.- TABULATED RESULTS OF DROPLET-TRAJECTORY DATA - Continued

(b) $C_L = 2.2$; $z_0 = 0.5$ semispan

y_0, semispans	y_g, semispans (*)	δ, microns	v_{d_g}, ft/sec	w_{d_g}, ft/sec	t_g, sec
0.25	0.692	150	2.56	-1.36	3.72
.25	.556	210	2.71	-2.06	2.61
.25	.480	275	2.76	-2.98	2.03
.25	.415	375	2.76	-4.26	1.54
.25	.370	500	2.72	-5.97	1.23
.25	.330	700	2.46	-8.91	.94
.50	(**)	150	-----	-----	----
.50	1.290	210	15.14	-2.45	1.86
.50	1.025	275	11.51	-3.16	1.52
.50	.855	375	8.79	-4.53	1.25
.50	.750	500	7.64	-5.67	1.02
.50	.653	700	6.26	-9.64	.76
.625	2.305	210	6.16	-1.93	3.51
.625	1.430	275	15.00	-2.68	1.45
.625	1.095	375	13.90	-4.54	1.06
.625	.940	500	11.60	-6.57	.87
.625	.815	700	9.11	-10.10	.67
.75	(**)	210	-----	------	----
.75	2.210	275	5.94	-2.42	3.11
.75	1.475	375	14.03	-3.59	1.18
.75	1.155	500	14.92	-6.23	.75
.75	.985	700	12.64	-10.40	.65

*The y_g values are without cross wind. To account for a cross wind, the product of t_g and the cross-wind velocity component may be applied as a correction to the tabulated y_g values.

**Computations were discontinued before droplet intersected ground plane.

TABLE III.- TABULATED RESULTS OF DROPLET-TRAJECTORY DATA - Concluded

(c) $C_L = 1.2$; $z_0 = 1.0$ semispan

y_0, semispans	y_g, semispans (*)	δ, microns	v_{dg}, ft/sec	w_{dg}, ft/sec	t_g, sec
0.25	1.750	150	6.56	-1.13	6.55
.25	.851	210	5.36	-2.12	4.47
.25	.500	375	3.01	-4.21	2.35
.25	.360	700	1.97	-8.81	1.75
.50	(**)	150	----	-----	----
.50	1.925	210	4.16	-1.90	5.60
.50	1.070	375	6.29	-4.08	2.74
.50	.740	700	4.21	-8.58	1.70

*The y_g values are without cross wind. To account for a cross wind, the product of t_g and the cross-wind velocity component may be applied as a correction to the tabulated y_g values.

**Computations were discontinued before droplet intersected ground plane.

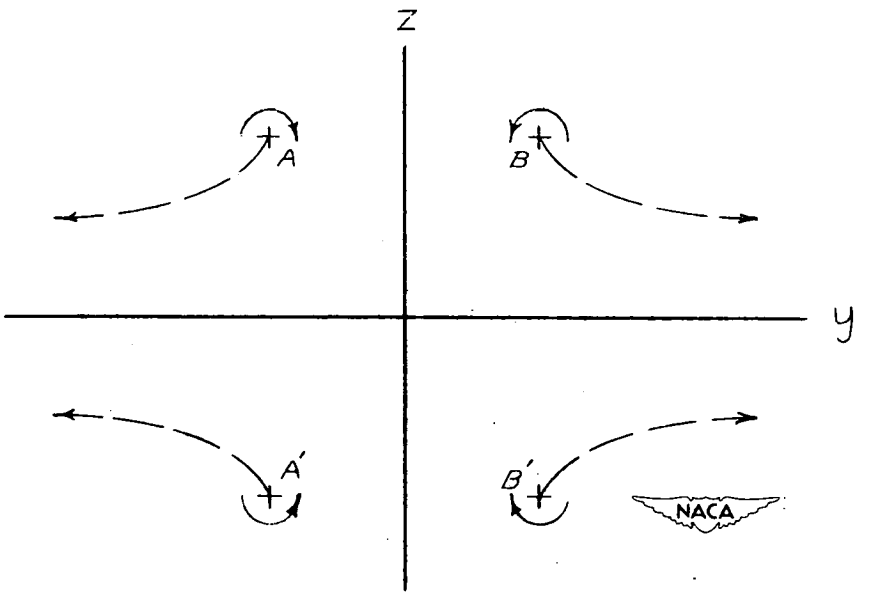

Figure 1.- Paths taken by the trailing vortices in the presence of a ground plane.

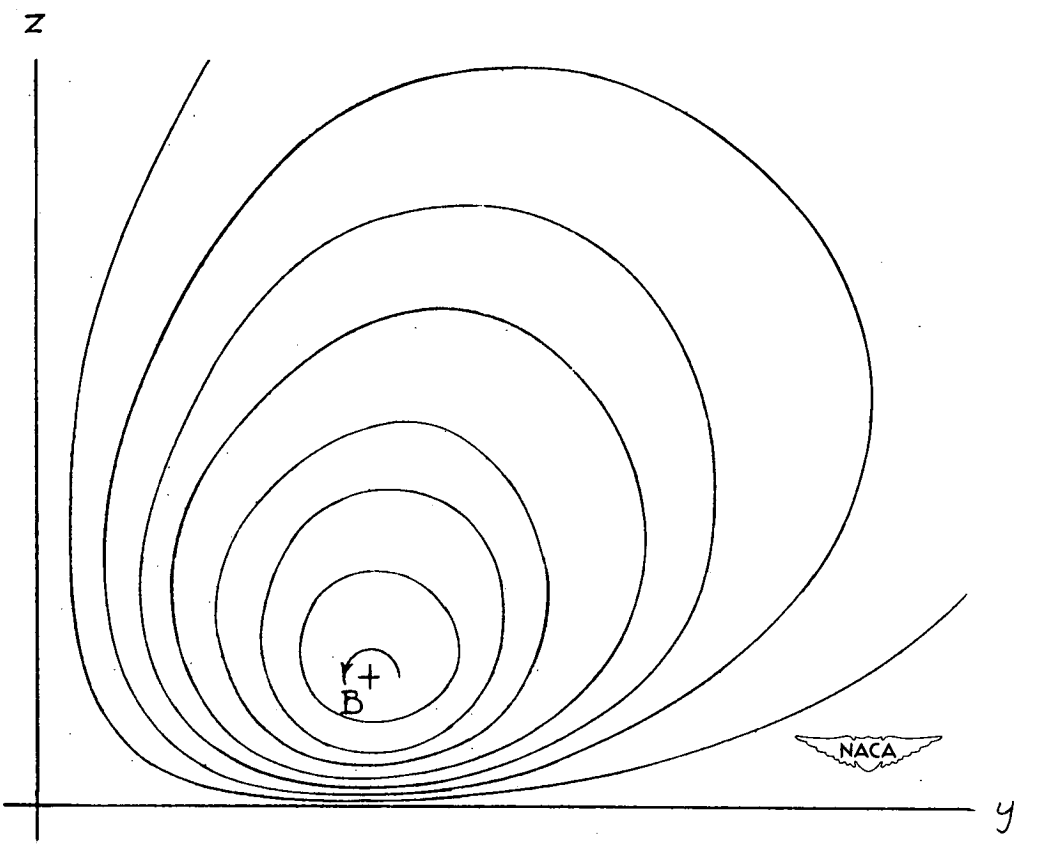

Figure 2.- Streamlines induced by the trailing vortices in the presence of a ground plane.

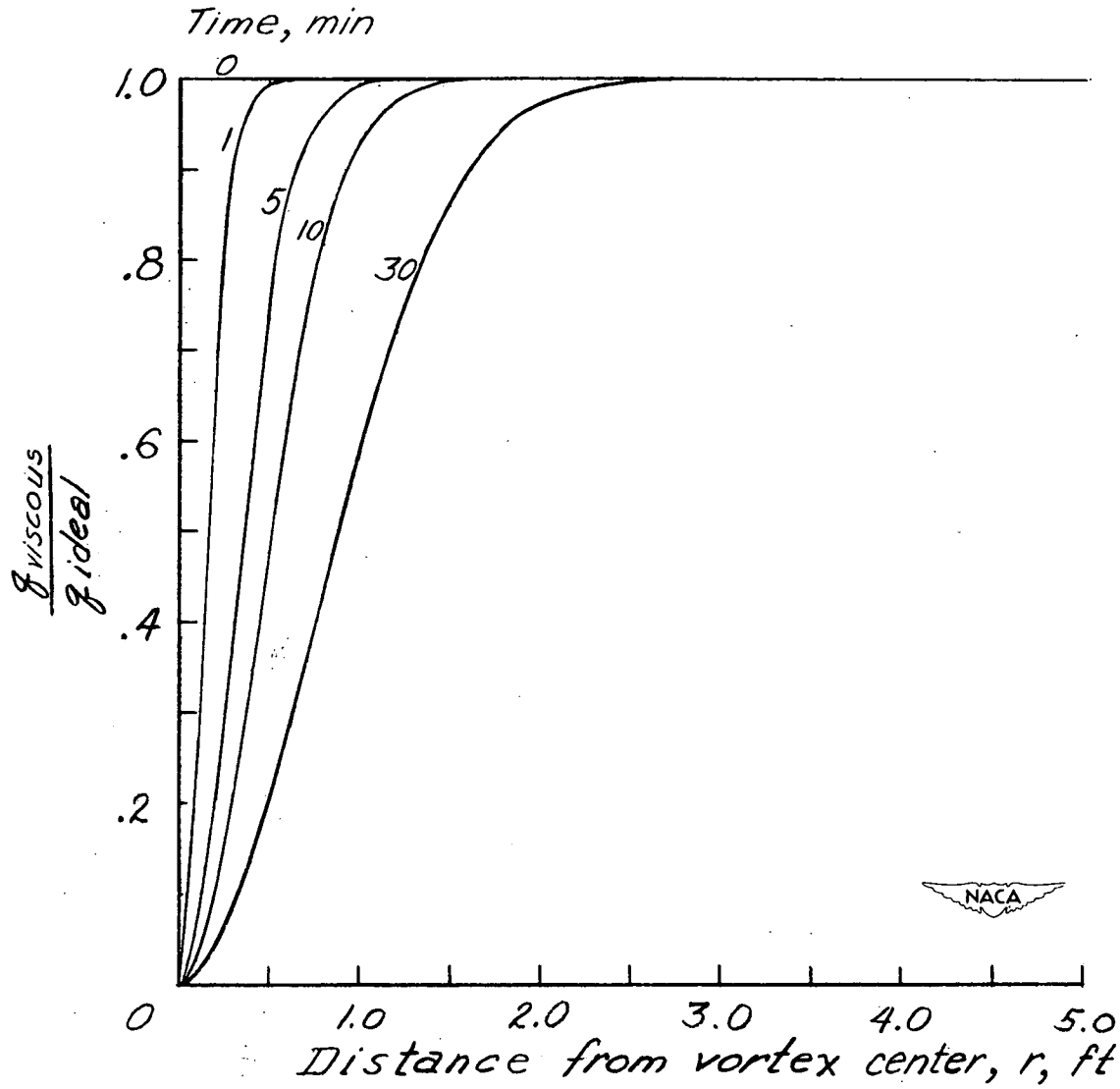

Figure 3.- Effect of viscosity on the reduction of velocity induced by an isolated rectilinear vortex as a function of time and distance from the core.

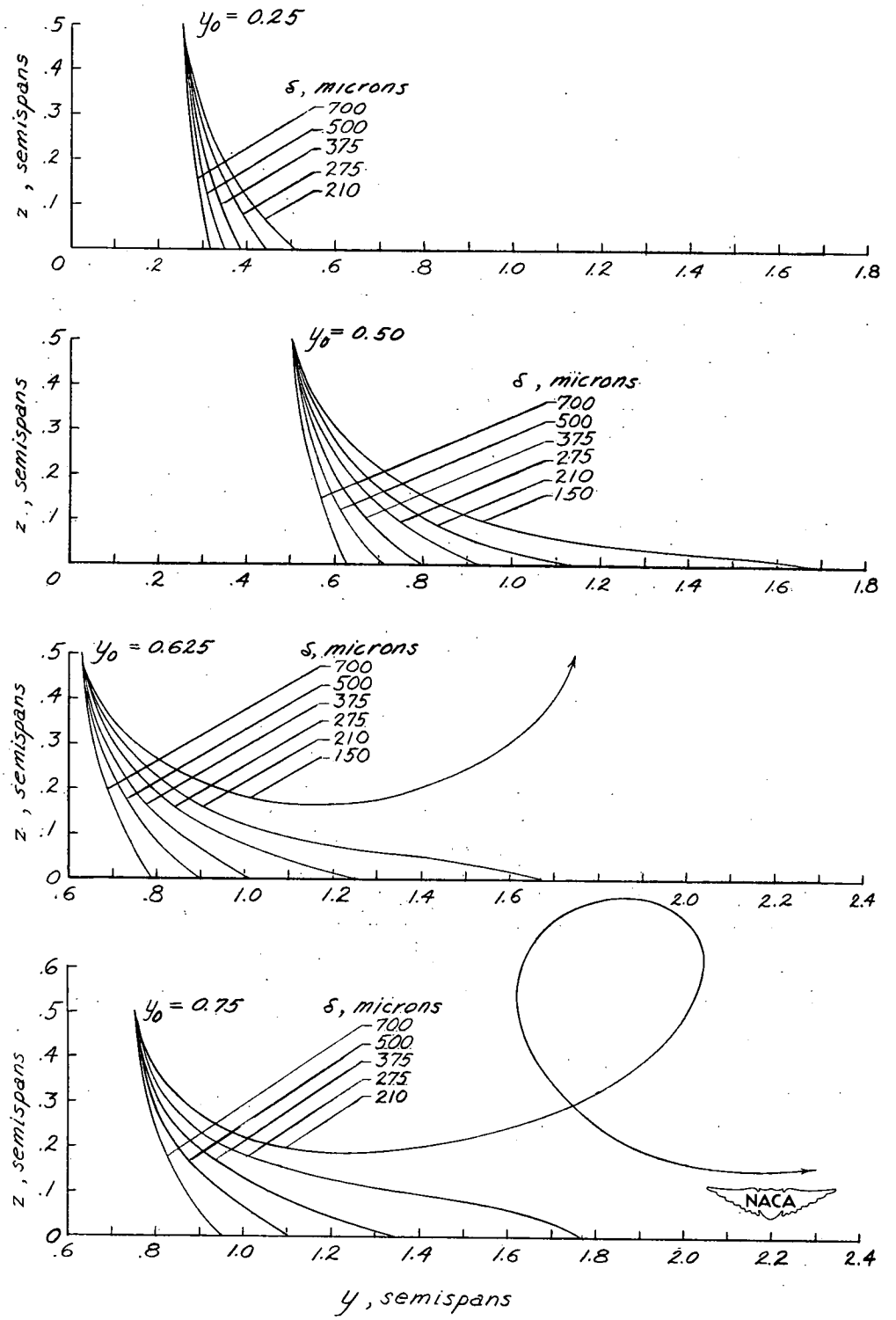

(a) $C_L = 1.2$; $z_0 = 0.5$ semispan.

Figure 4.- Calculated trajectories of spray droplets ejected from an airplane.

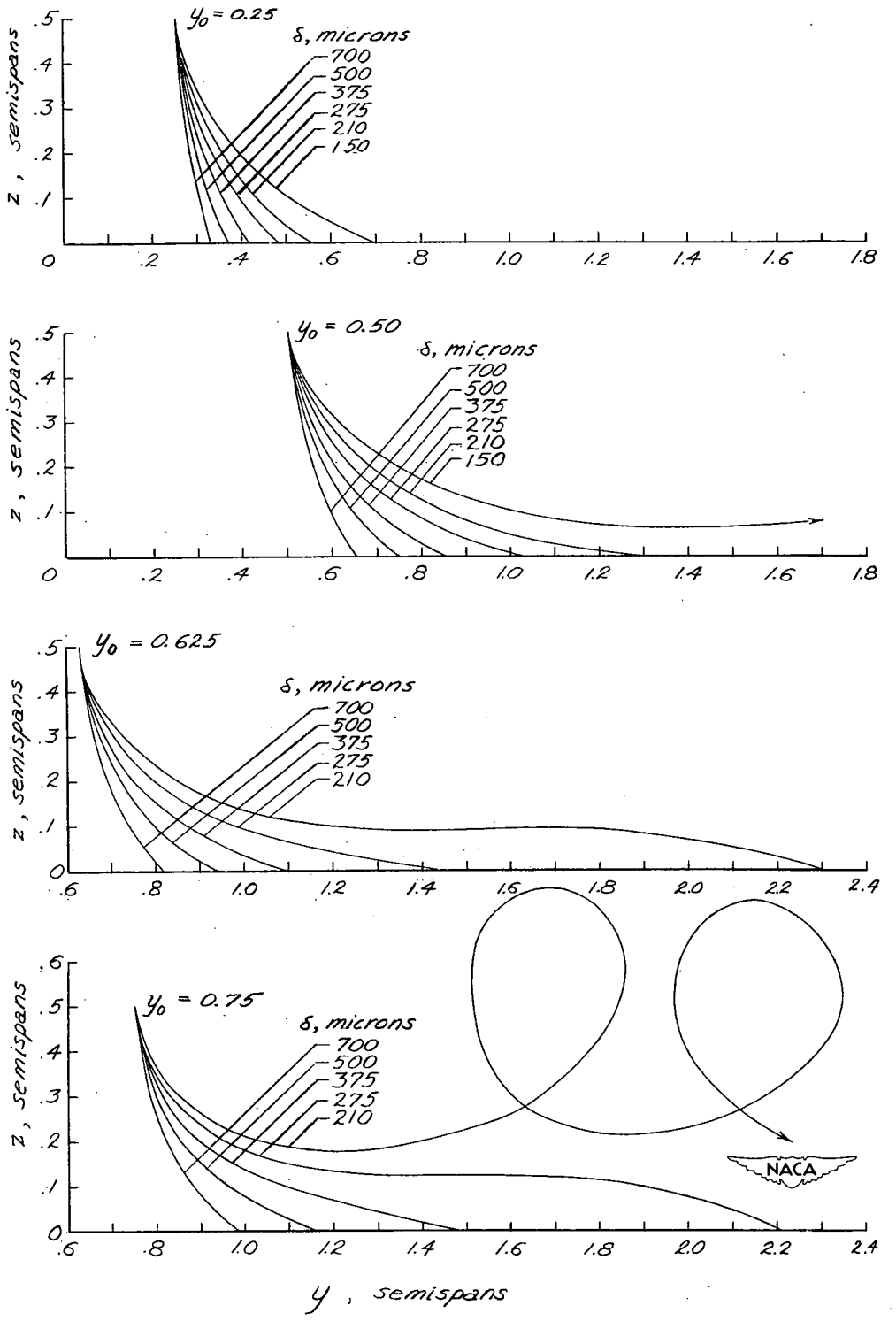

(b) $C_L = 2.2$; $z_0 = 0.5$ semispan.

Figure 4.- Continued.

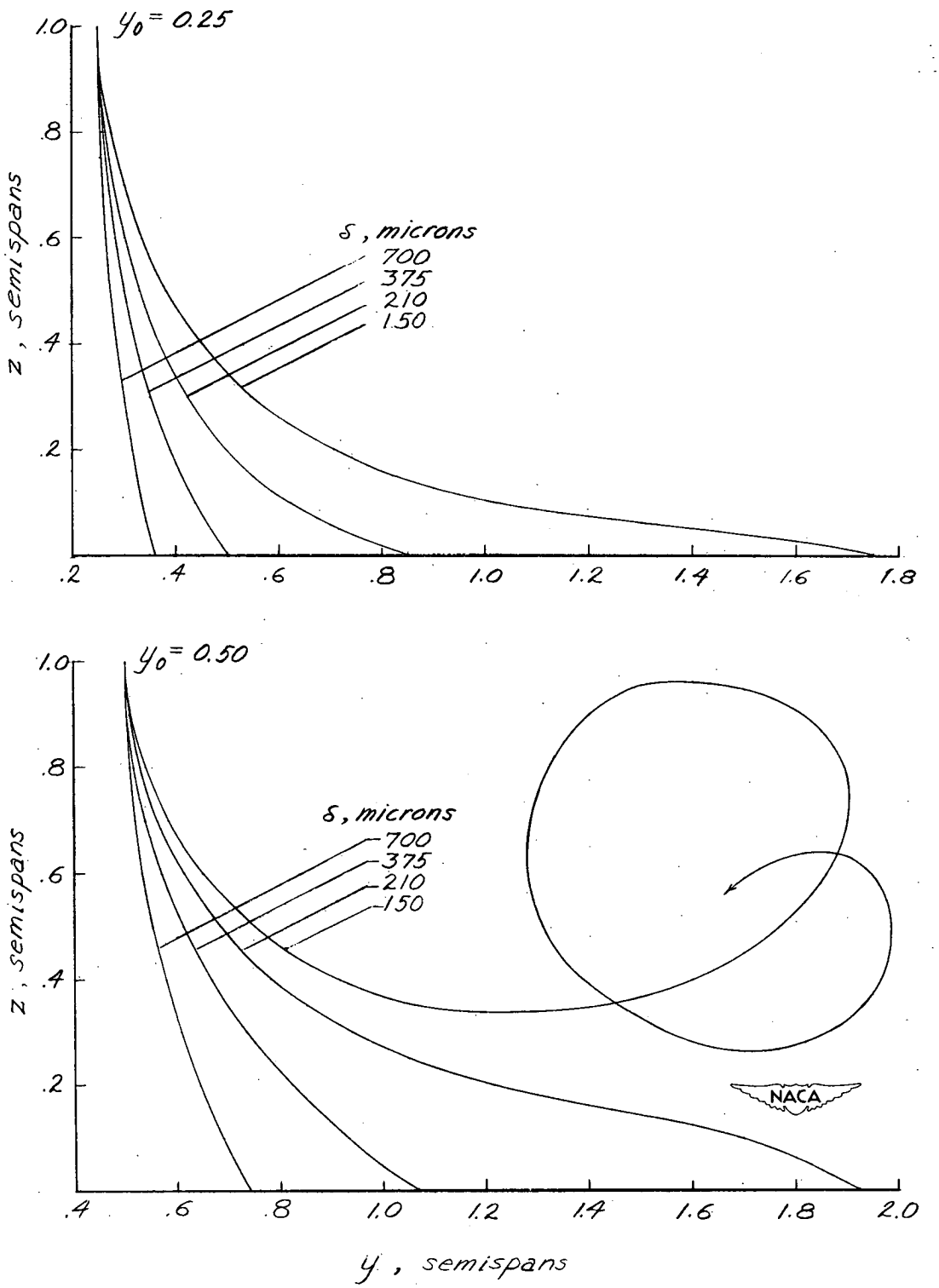

(c) $C_L = 1.2$; $z_0 = 1.0$ semispan.

Figure 4.- Concluded.

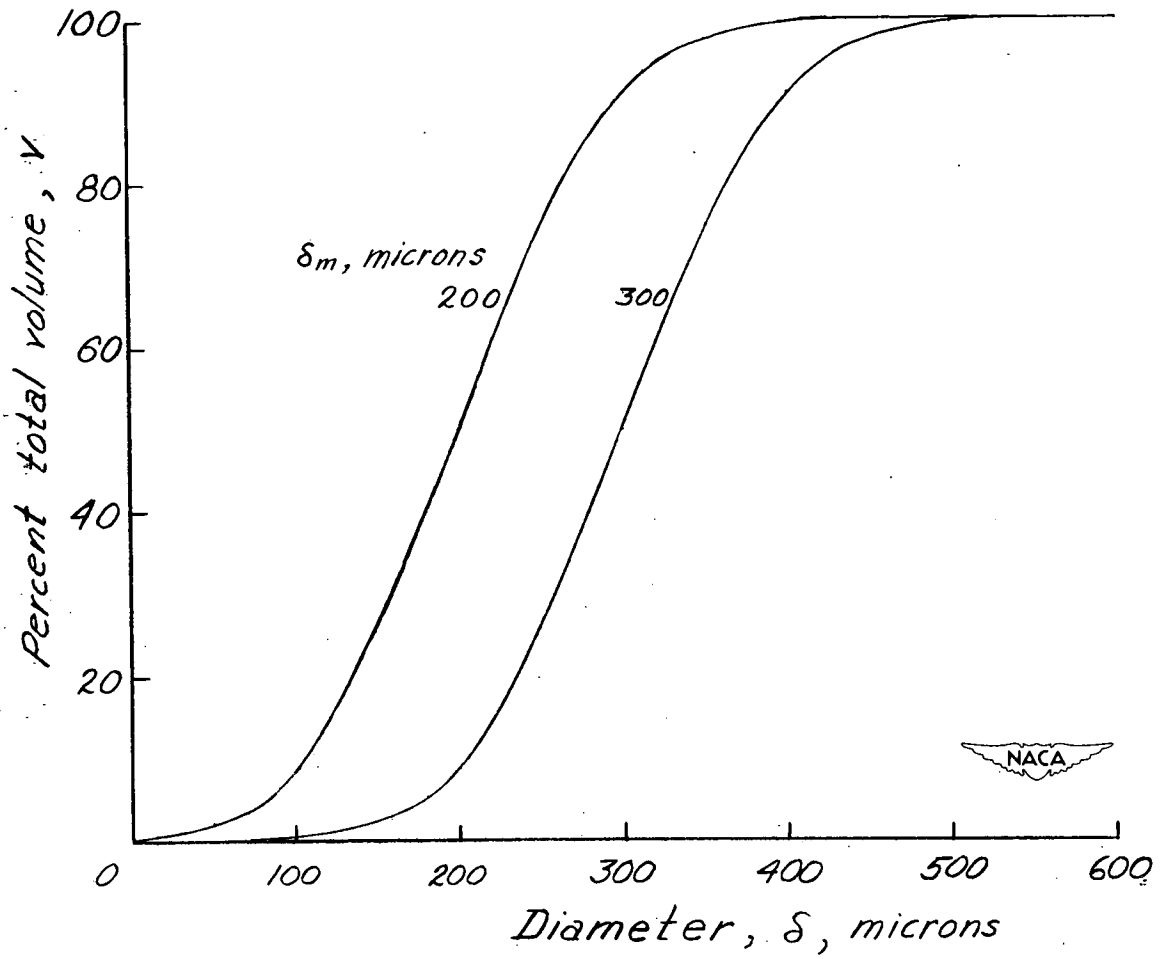

Figure 5.- Sample droplet-size spectra used in analysis.

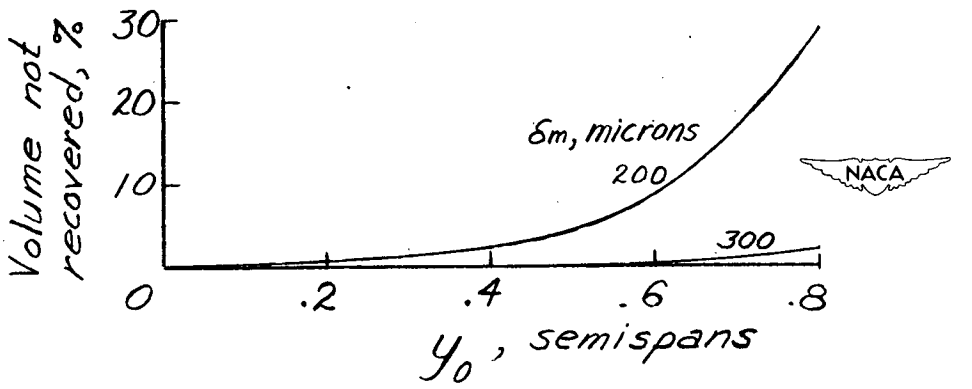

Figure 6.- Percentage of volume not recovered in deposit as a function of spanwise starting position for $C_L = 1.2$ and $z_0 = 0.5$ semispan.

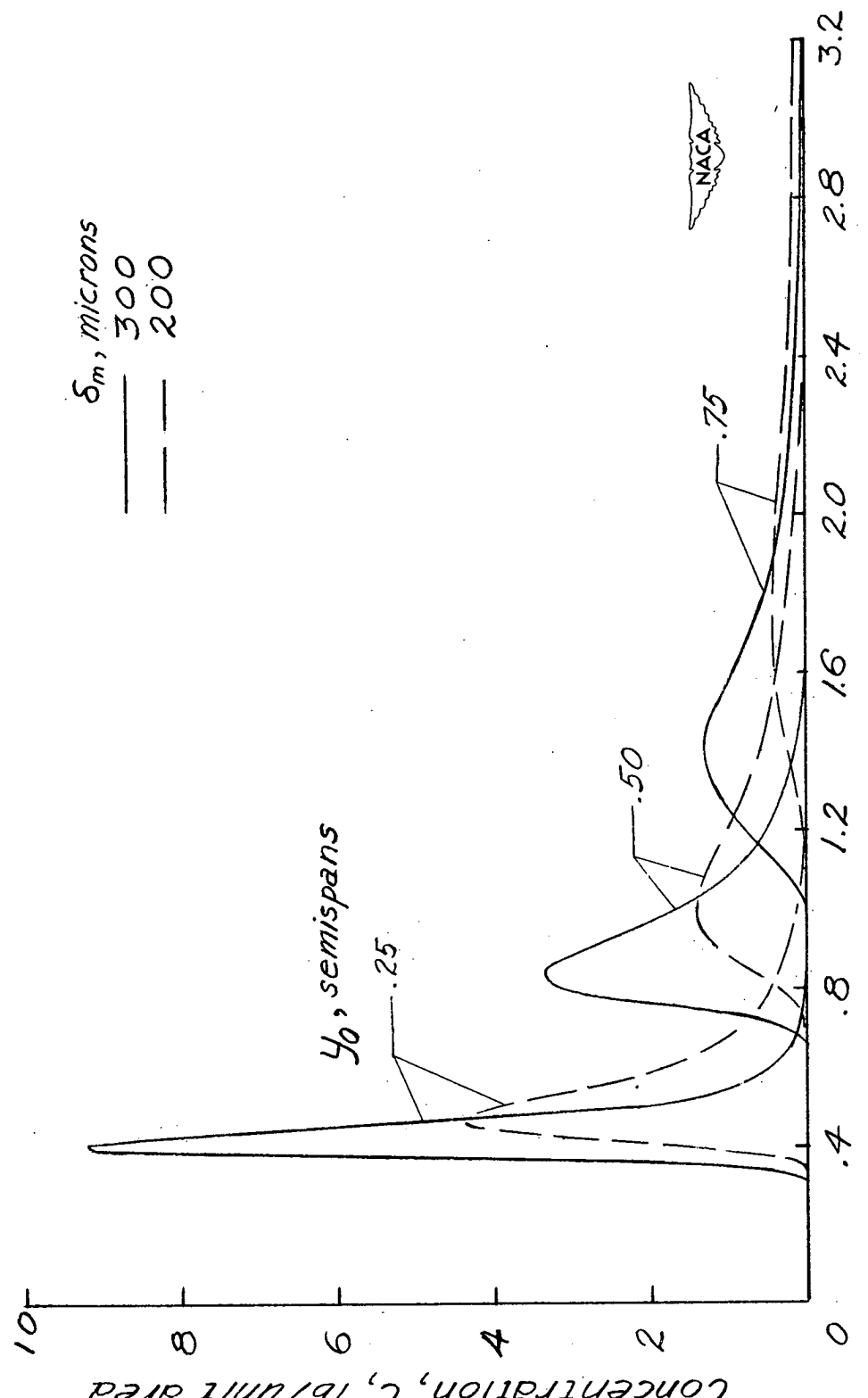

Figure 7.- Effect of the mean droplet diameter on distribution of deposit for discrete nozzles. C_L = 1.2; z_0 = 0.5 semispan.

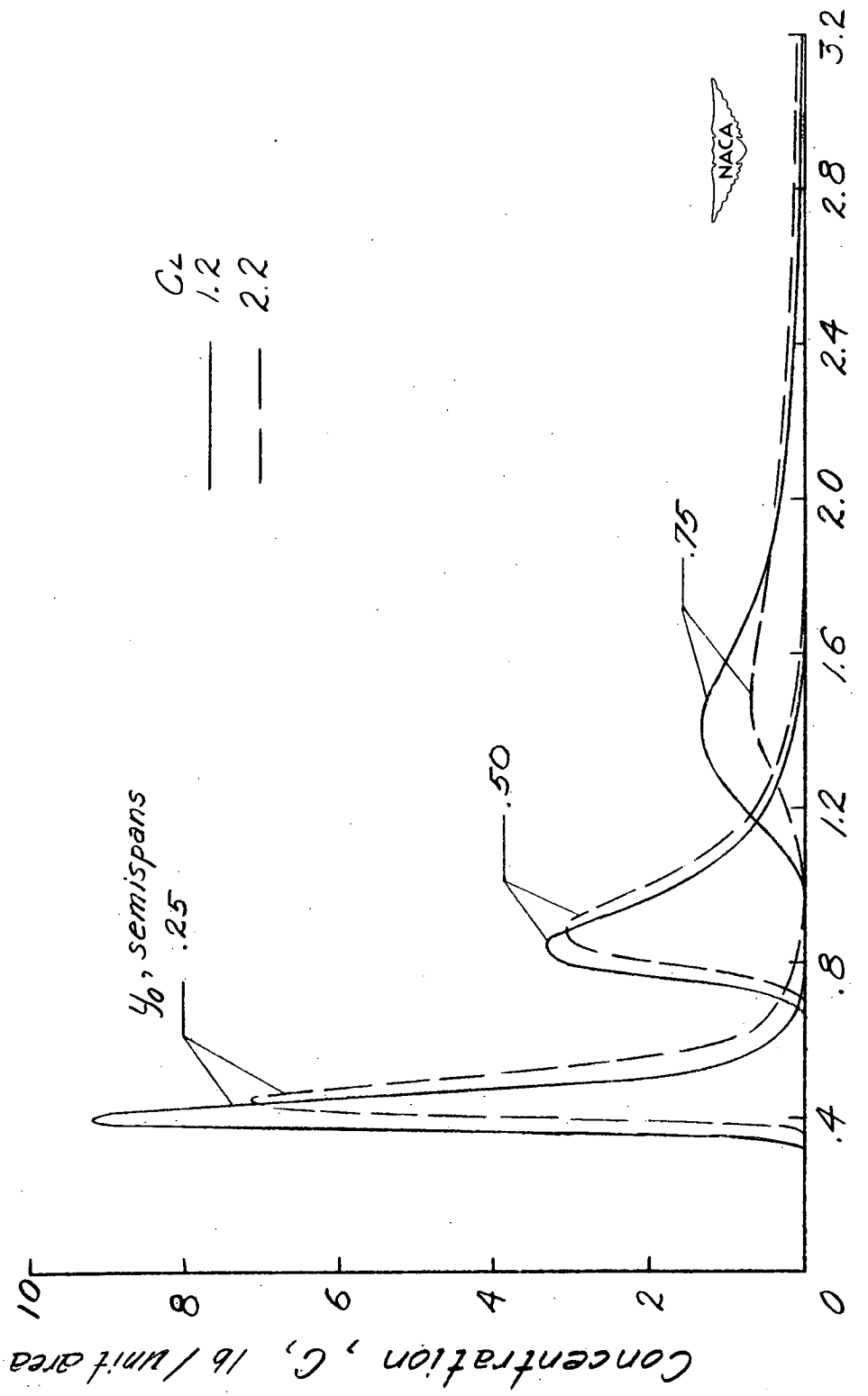

Figure 8.- Effect of airplane lift coefficient on distribution of deposit for discrete nozzles. z_0 = 0.5 semispan; δ_m = 300 microns.

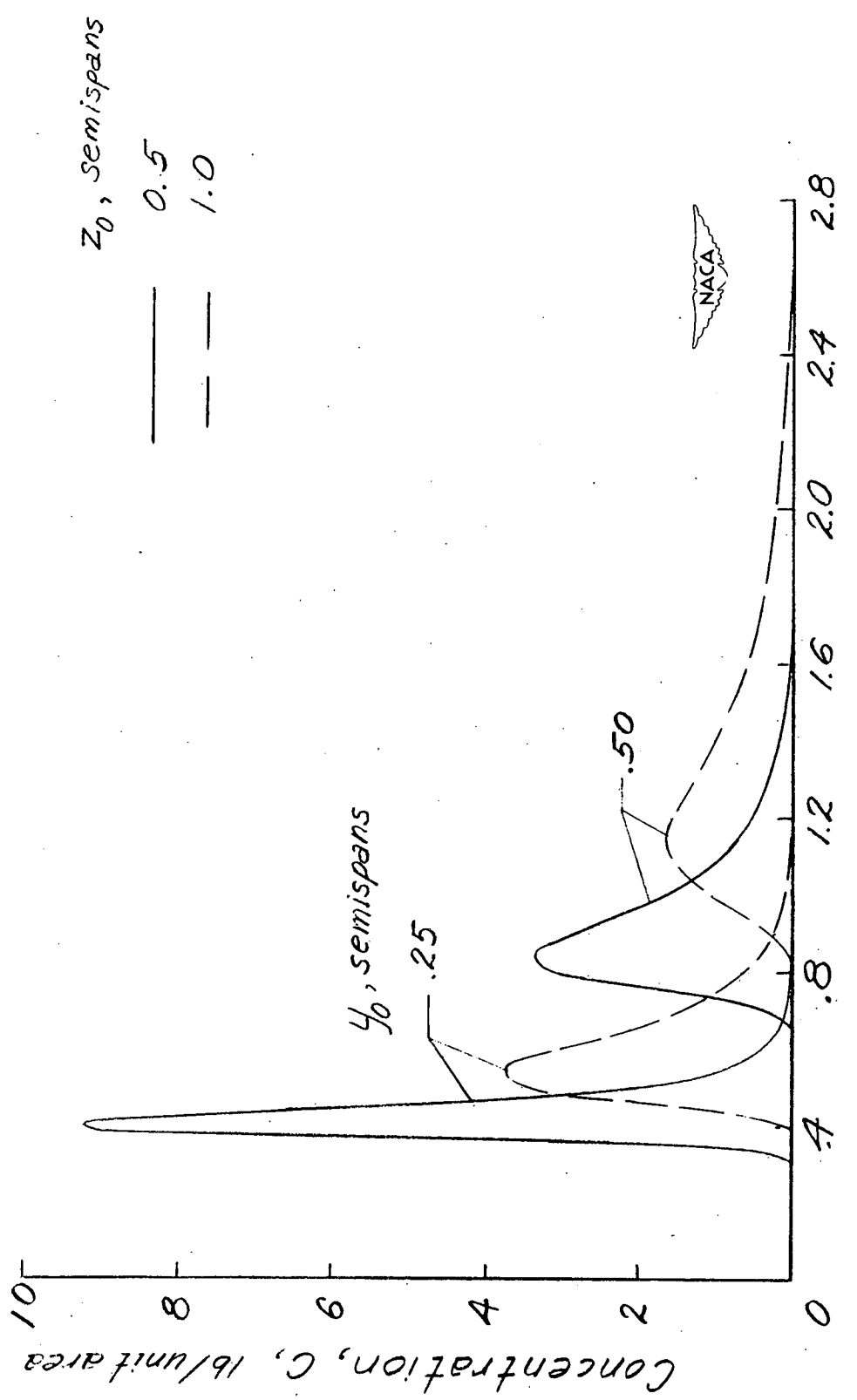

Figure 9.- Effect of airplane height on distribution of deposit for discrete nozzles. $C_L = 1.2$; $\delta_m = 300$ microns.

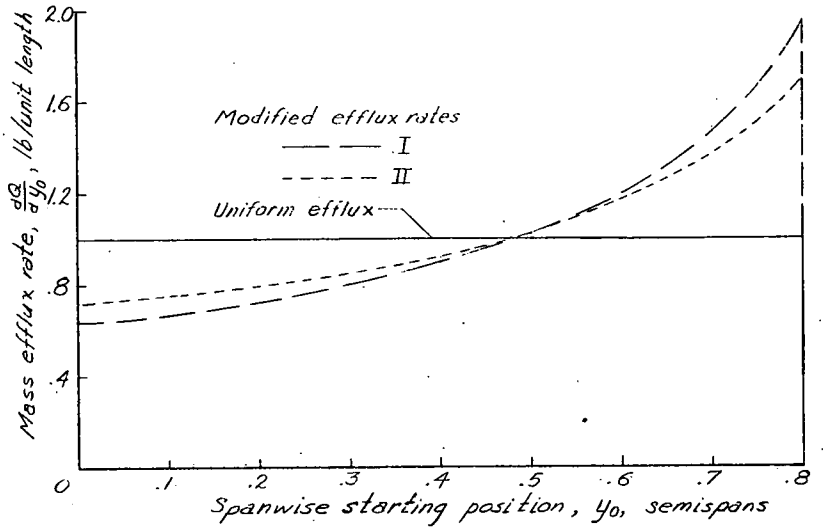

(a) Mass efflux rate variations.

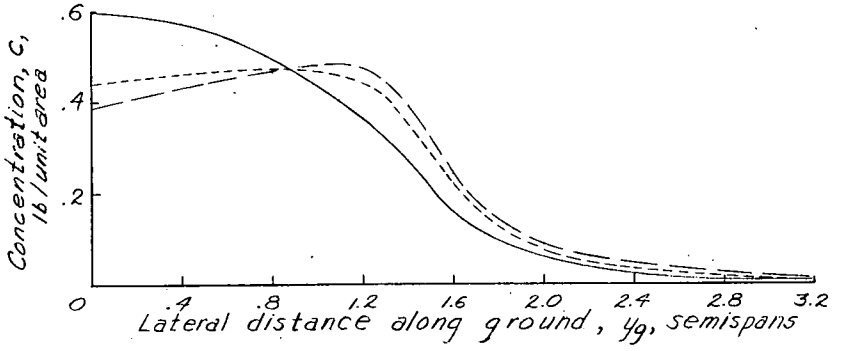

(b) Deposit curves; δ_m = 300 microns.

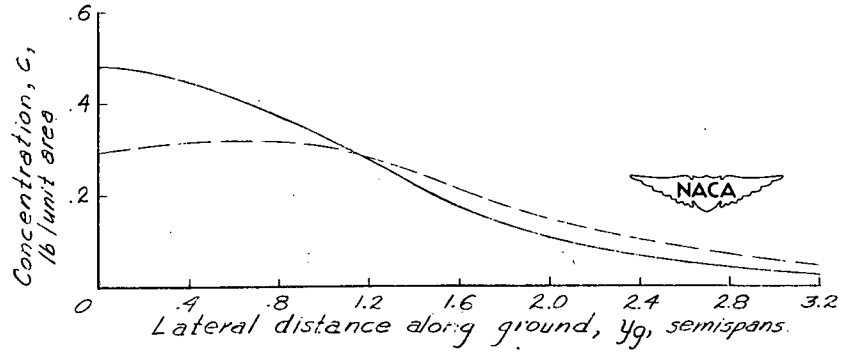

(c) Deposit curves; δ_m = 200 microns.

Figure 10.- Effect of spanwise variations of a continuous mass efflux rate on distribution of deposit. C_L = 1.2; z_0 = 0.5 semispan.

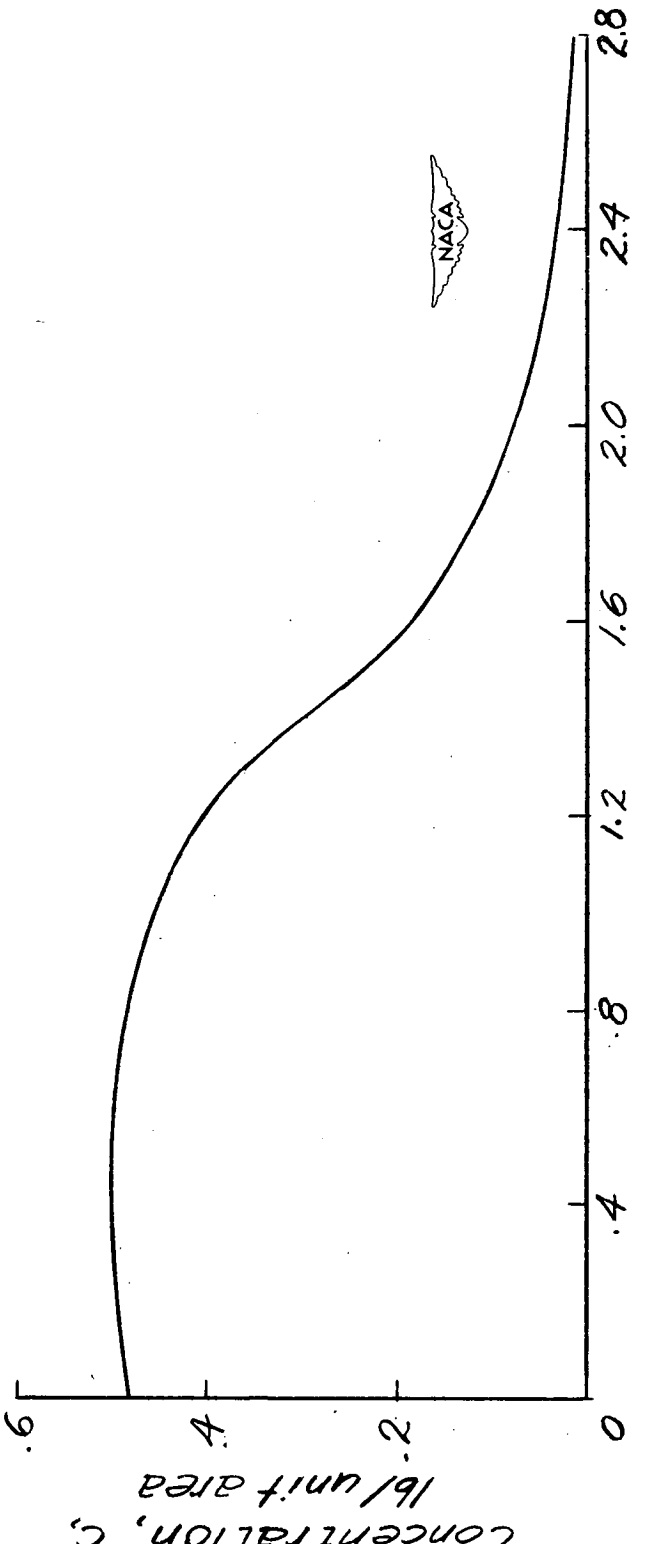

Figure 11.- Distribution of deposit with a linear spanwise increase in the mean diameter of the droplet-size spectrum. $\delta_m = 200 + 125y_0$;

$C_L = 1.2$; $z_0 = 0.5$ semispan; $\frac{dQ}{dy_0} = 1.0$.

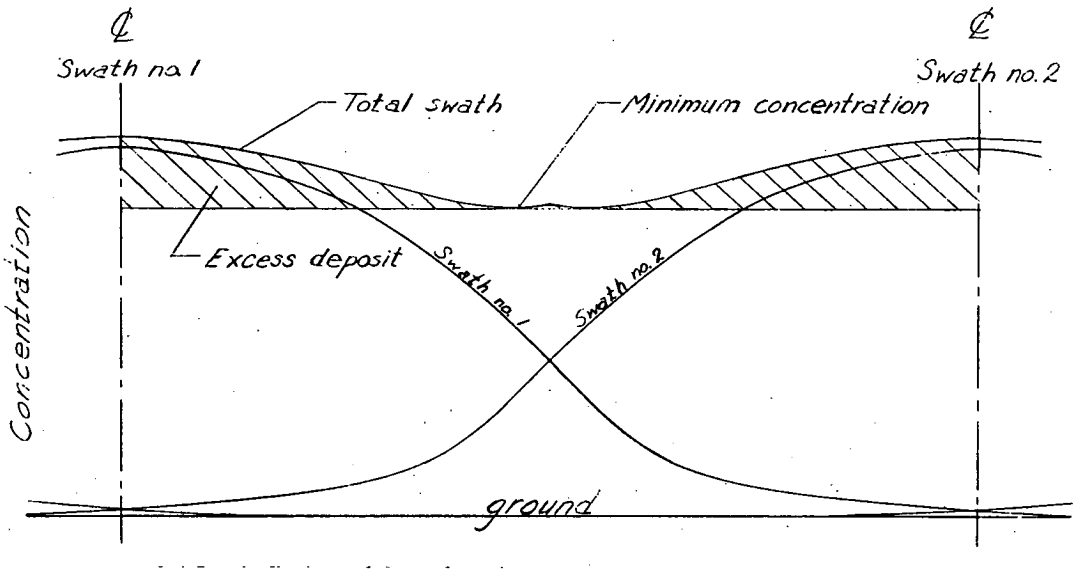

(a) Overlapping of adjacent swaths.

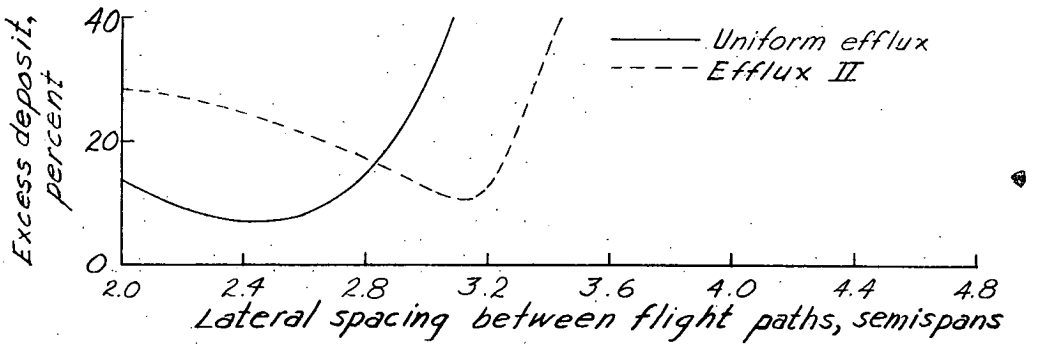

(b) δ_m = 300 microns.

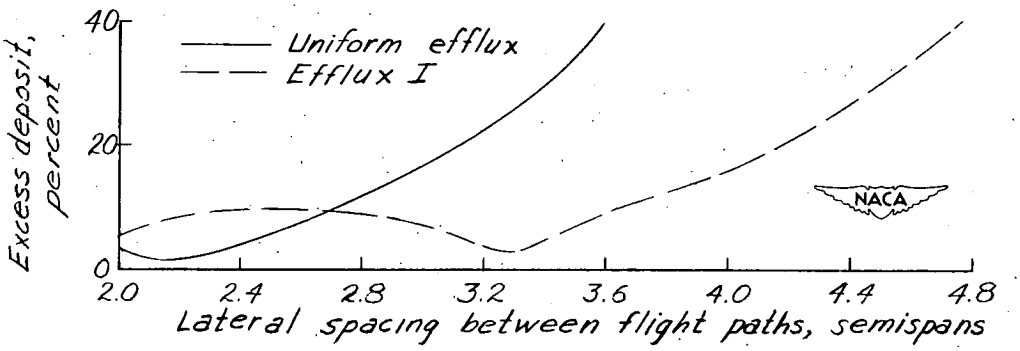

(c) δ_m = 200 microns.

Figure 12.- Illustration of the excess deposit of overlapping swaths and its variation with flight-path spacing.

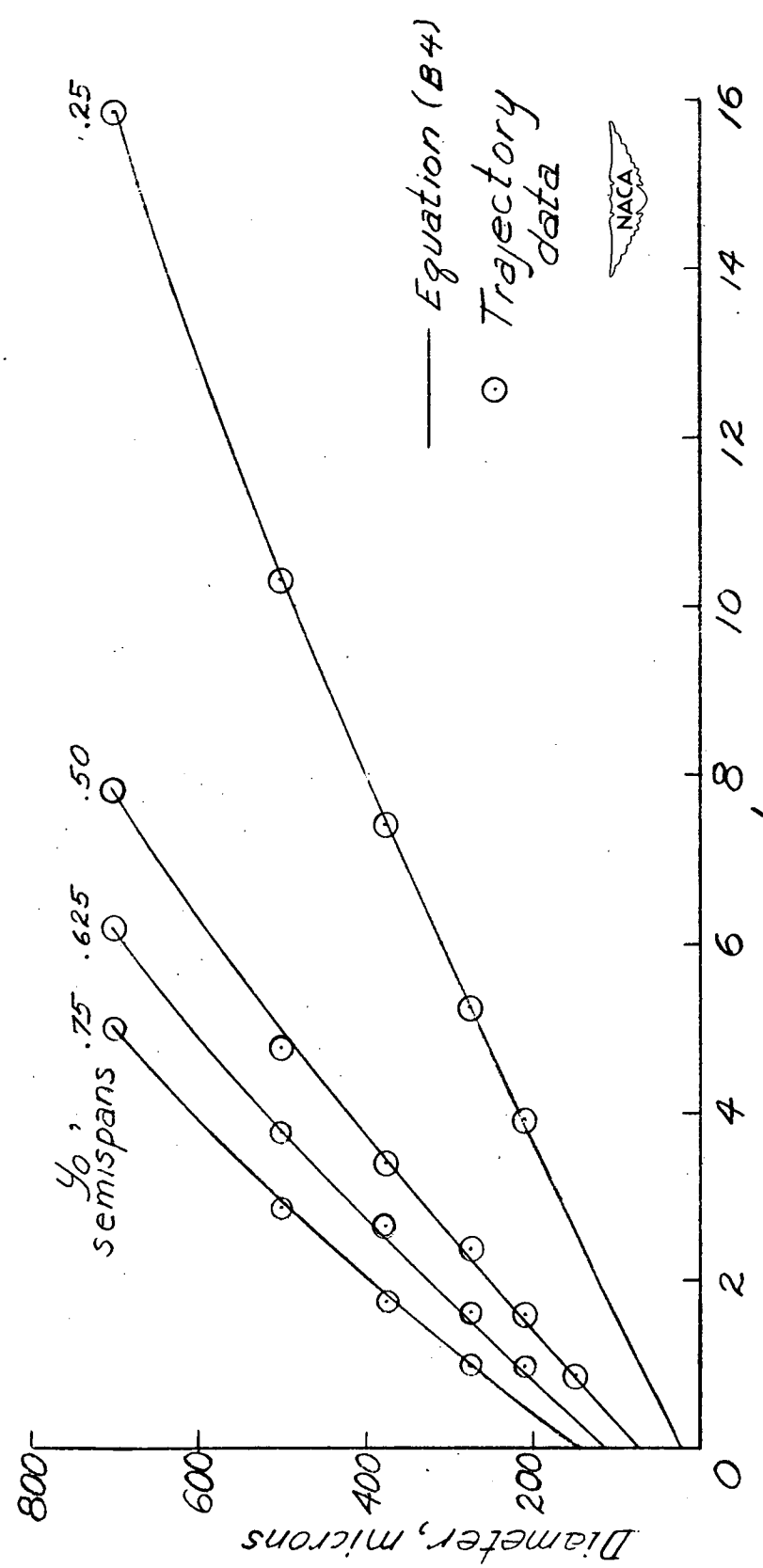

Figure 13.- Empirical representation of droplet diameter as a function of y_0 and y_g. $C_L = 1.2$; $z_0 = 0.5$.